

PDZ-directed substrate recruitment is the primary determinant of specific 4E-BP1 dephosphorylation by PP1-Neurabin

Roman O Fedoryshchak, Karim El-Bouri, Dhira Joshi, Stephane Mouilleron, Richard Treisman 

Signalling and transcription Laboratory, Francis Crick Institute, London, UK • Structural Biology STP, Francis Crick Institute, London, UK • Chemical Biology STP, Francis Crick Institute, London, UK

 https://en.wikipedia.org/wiki/Open_access

 Copyright information

eLife Assessment

This **important** study reports on a basis for neurabin-mediated specification of substrate choice by protein phosphatase-1. The data from the comprehensive approach using structural, biochemical, and computational methods are **compelling**, but the role of the crucial tryptophan residue in the recognition motif can be further tested to strengthen the main argument. This paper is broadly relevant to those investigating various cellular signaling cascades that entail phosphorylation as the main mechanism.

<https://doi.org/10.7554/eLife.103403.1.sa4>

Abstract

Protein Phosphatase 1 (PP1) relies on association with PP1-interacting proteins (PIPs) to generate substrate-specific PIP/PP1 holoenzymes, but the lack of well-defined substrates has hindered elucidation of the mechanisms involved. We previously demonstrated that the Phactr1 PIP confers sequence specificity on the Phactr1/PP1 holoenzyme by remodelling the PP1 hydrophobic substrate groove. Phactr1 defines a group of “RVxF-ΦΦ-R-W” PIPs that all interact with PP1 in a similar fashion. Here we use a PP1-PIP fusion approach to address sequence specificity and identify substrates of the RVxF-ΦΦ-R-W family PIPs. We show that the four Phactr proteins confer identical sequence specificities on their holoenzymes. We identify the 4E-BP and p70 S6K translational regulators as substrates for the Neurabin/Spinophilin PIPs, implicated in neuronal plasticity, pointing to a role for their holoenzymes in mTORC1-dependent translational control. Biochemical and structural experiments show that in contrast to the Phactrs, substrate recruitment and catalytic efficiency of the PP1-Neurabin and PP1-Spinophilin fusions is primarily determined by substrate interaction with the PDZ domain adjoining their RVxF-ΦΦ-R-W motifs, rather than by recognition of the remodelled PP1 hydrophobic groove. Thus, even PIPs that interact with PP1 in a similar manner use different mechanisms to ensure substrate selectivity.

Introduction

Protein Phosphatase 1 is a member of the PPP superfamily of protein phosphatases, responsible for most cellular serine/threonine dephosphorylation (Bollen et al, 2010 [↗](#); Brautigan and Shenolikar, 2018 [↗](#)) {Bollen, 2010 #4; Brautigan, 2018 #6}. The three PP1 isoforms possess a central metal-binding active centre from which radiate three putative substrate-binding grooves (Egloff et al, 1995 [↗](#); Goldberg et al, 1995 [↗](#)), but have little intrinsic sequence specificity (Hoermann et al, 2020 [↗](#)). Instead, PP1 substrate specificity and activity is controlled by over 200 PP1 interacting proteins (PIPs), which use a number of short linear motifs (SLIMs) to dock with distinct regions of the PP1 surface, including the substrate-binding grooves (Cohen, 2002 [↗](#); Bollen et al., 2010 [↗](#); Casamayor and Arino, 2020 [↗](#)). PIPs can target PP1 to specific subcellular locations, and are control substrate specificity through autonomous substrate-binding domains, occupation or extension of the substrate grooves, or modification of PP1 surface electrostatics (for references see Bollen et al., 2010 [↗](#); Fedoryshchak et al, 2020 [↗](#)). Only a few PIP-PP1-substrate interactions are understood in molecular detail, however, and the question of whether PIP interaction imposes sequence specificity on PP1, as opposed to simply bringing enzyme and substrate into close apposition, has remained largely unexplored.

The Phactr family of actin-regulated PP1 cofactors are the only PIPs known to directly impose substrate sequence-specificity at the dephosphorylation site itself (Fedoryshchak et al., 2020 [↗](#)). They belong to subset of PIPs that bind PP1 through a conserved “RVxF-ΦΦ-R-W string” (Ragusa et al, 2010 [↗](#); Choy et al, 2014 [↗](#); Chen et al, 2015 [↗](#); Fedoryshchak et al., 2020 [↗](#); Yan et al, 2021 [↗](#)). These include Neurabin/Spinophilin, which play important roles in PP1-dependent regulation of neuronal plasticity (Allen et al, 1997 [↗](#); Burnett, 1998 #87, reviewed by Sarrouilhe et al, 2006 [↗](#); Foley et al, 2021 [↗](#)); PNUTS, which regulates PolII and chromatin dynamics (Lee et al, 2010 [↗](#); Cortazar et al, 2019 [↗](#)); and PPP1R15A/B, which mediates translational regulation through control of eIF2 dephosphorylation (Novoa et al, 2001 [↗](#); Chen et al., 2015 [↗](#); Yan et al., 2021 [↗](#)). In the Phactr1-PP1 holoenzyme, Phactr1 sequences C-terminal to the RVxF-ΦΦ-R-W string interact with the PP1 hydrophobic groove to form a composite hydrophobic pocket, topped by a basic rim. This imposes strong sequence selectivity on substrates, favouring hydrophobic residues at positions +4/+5 relative to the phosphorylated residue, within an acidic context (consensus pS/T-x₍₂₋₃₎-Δ-L, the “LLD motif”). Strikingly, this specificity is maintained in a PP1-Phactr1 fusion protein comprising PP1(1-304) linked to Phactr1 sequences from residue 526, just C-terminal to its RVxF motif.

Neurabin/Spinophilin remodel the PP1 hydrophobic groove differently from Phactr1, generating a structurally distinct surface on the holoenzyme (Ragusa et al., 2010 [↗](#); Fedoryshchak et al., 2020 [↗](#)), and it is likely that the other RVxF-ΦΦ-R-W PIPs do so as well. Whether and how these diverse surfaces might play a role in the substrate specificity of these PIP/PP1 holoenzymes has remained unclear, largely because little is known about their substrates. Here we investigate determinants of substrate specificity in the other RVxF-ΦΦ-R-W PIPs, focussing on Neurabin/Spinophilin, which also contain a PDZ domain previously suggested to be involved in substrate recruitment (Burnett et al, 1998 [↗](#); Kelker et al, 2007 [↗](#)). We use the PP1-PIP fusion approach to show that the four Phactr1 holoenzymes have indistinguishable substrate specificities, and to identify novel candidate substrates for the other RVxF-ΦΦ-R-W PIP/PP1 complexes. We use 4E-BP1, a new Neurabin/PP1 substrate, to show that unlike the Phactr1/PP1 holoenzyme, substrate specificity of Neurabin/PP1 is largely determined by interaction with the Neurabin PDZ domain rather than the primary sequences of the dephosphorylation site itself.

Results

PP1-PIP fusion proteins

The PP1 C-terminal sequences closely approach the Phactr1 RVxF-ΦΦ-R-W string in the vicinity of the ΦΦ motif, which allowed the construction of a single chain PP1α-PIP fusion derivative comprising PP1α(7-304) linked to Phactr1 sequences from a point just C-terminal to its RVxF motif (**Figure 1A**). The remodelled hydrophobic groove of this fusion is structurally identical to that of the Phactr/PP1 holoenzyme, and it retains similar activity and specificity (Fedoryshchak et al., 2020). Guided by the structures of the other RVxF-ΦΦ-R-W PIPs, we generated analogous fusions of N-terminally Flag-tagged PP1 with fragments of Neurabin and Spinophilin (PPP1R9A/B, Bollen et al., 2010), PPP1R15A and PPP1R15B (Chen et al., 2015), and PNUTS (PPP1R10, Choy et al., 2014), comprising the PP1-interacting sequences and any known protein interaction domains immediately C-terminal to them. We also constructed fusions with each the four Phactr proteins to explore any variation in their sequence specificities (**Figure 1A, 1B**; **Figure S1A**).

Each fusion protein was stably expressed in 293 Flp-In T-Rex cells using a tetracycline-inducible vector (Ward et al., 2011). Tetracycline titration of PP1-Phactr1 cells induced increasing expression of the fusion protein, leading to corresponding dephosphorylation of its substrates IRSp53 pS455 and Afadin pS1275 (Fedoryshchak et al., 2020) (**Figure 1B**). Afadin pS1275 was also dephosphorylated by the other three PP1-Phactr fusions, but not by the other PP1-PIP fusions (**Figure 1C**). Similar results were observed with exogenously expressed wildtype IRSp53; as expected, the +5 residue L460A mutation, which impairs dephosphorylation by the intact Phactr1/PP1 holoenzyme, impaired sensitivity to all the fusions, indicating that they recognise phosphorylated IRSp53 in a similar way (**Figure S1B**).

Proteomic analysis of PP1-fusion specificity

To investigate the substrate specificities of the fusion proteins, we performed Tandem-Mass-Tag (TMT) phosphoproteomics. Fractionated peptides were measured in both MS2 and MS3 modes for maximal identification and quantification (**Figure 2A**). Phosphorylation site abundances within triplicate samples from the same cell line were comparable between replicates (**Figure 2B**). First, we identified phosphorylation sites significantly depleted by expression of PP1α(7-304) alone compared with vector only, using Perseus software and a t-test with a 1% permutation-based false-discovery rate cutoff (Tyanova et al., 2016). In agreement with previous results (Hoermann et al., 2020), PP1 exhibited little sequence specificity, other than a preference for positively charged residues in positions -3, -1 and +3 to the dephosphorylation site (**Figure S2A**, **S2B**).

We then compared the specificities of the four PP1-Phactr fusion proteins. Expression of the PP1-Phactr1 revealed numerous phosphorylation sites that were specifically depleted compared with cells expressing PP1α alone (**Figure 2C**). This population contained Phactr1/PP1 holoenzyme substrates previously identified in neurons or NIH3T3 fibroblasts (Fedoryshchak et al., 2020), including IRSp53 pS455 and Afadin pS1275, and was substantially enriched in the Phactr1/PP1 consensus dephosphorylation motif S/T-x_{2,3}-Φ-L (**Figure 2D**). The profiles of PP1-Phactr2, PP1-Phactr3, and PP1-Phactr4 cells were substantially similar (**Figure S2C**), exhibiting good overall correlations both between total phosphorylation site profiles (**Figure 2B**), and significant enrichment for both the S/T-x_{2,3}-Φ-L motif and specific Phactr1/PP1 substrates (**Figure 2D**); over 60% of the depleted phosphorylation sites were in common between all four fusions (**Figure 2E**). These data show that the PP1-Phactr fusions recapitulate the specificity of the Phactr1/PP1 holoenzyme.

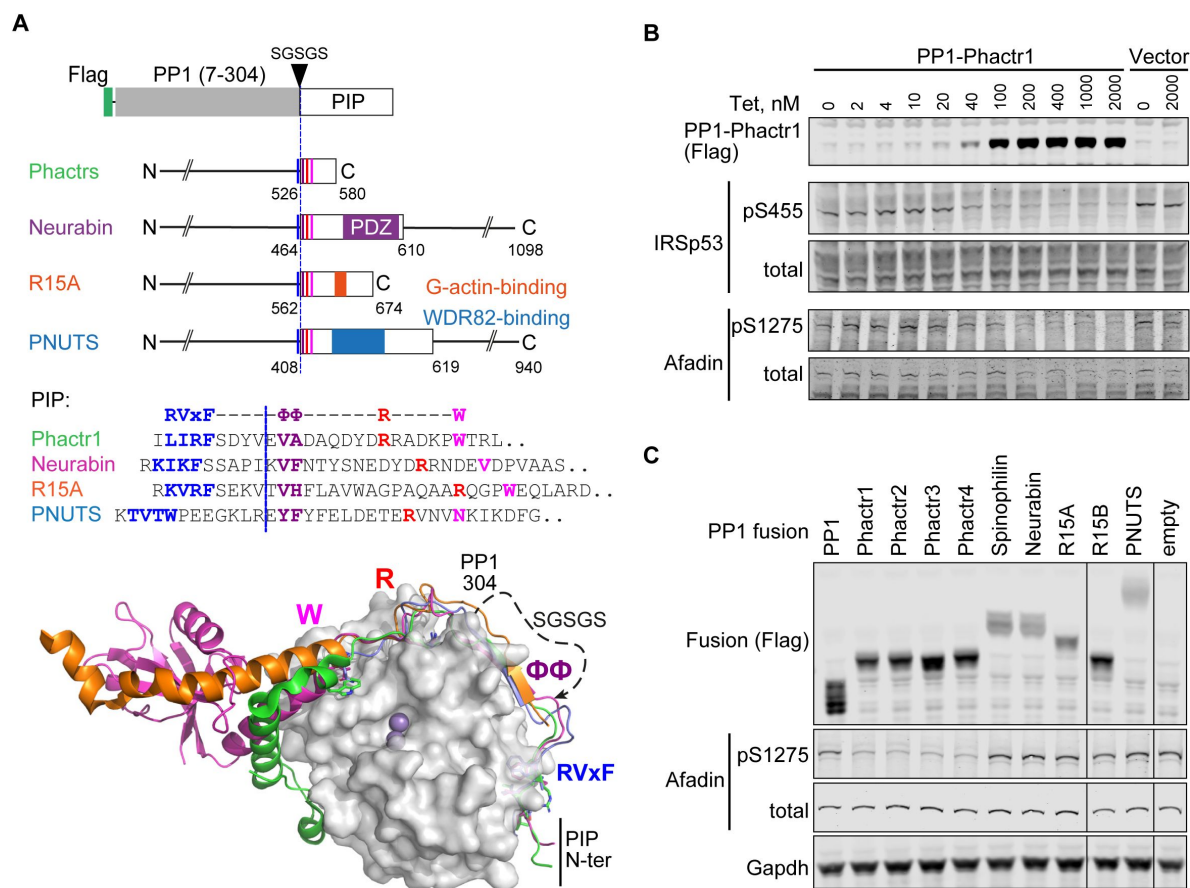


Figure 1.

PP1-PIP fusion proteins.

A. Structures of fusion proteins. N-terminally Flag-tagged PP1α(7-304) is linked to sequences from each of the four families of RVxR-ΦΦ-R-W PIPs, shown as an open box. Each fusion contains sequences immediately C-terminal to the PP1 interaction motif (coloured lines) including known protein interaction domains previously implicated in potential substrate interactions (coloured blocks). For PIP sequences in each fusion see [Figure S1A](#) and Methods.

Middle, sequences of the RVxR-ΦΦ-R-W string in each PIP, with motifs coloured. Each fusion contains the sequences C-terminal to the dashed line, represents the position of PP1-SGSGS linker insertion.

Bottom, structures of PP1/PIP complexes. Crystal structures of different PIP/PP1 complexes superimposed, aligned on PP1. Grey: PP1 (PDB: 4MOV), with PIP sequences as follows: green, Phactr1 (PDB: 6ZEE); magenta, Neurabin (PDB: 3HVQ); orange, R15A (PDB: 7NZM); blue, PNUTS (PDB: 4MOY). Dashed line, SGSGS linker.

B. Activity of PP1-Phactr1 expressed in Flp-In T-Rex 293 cells. PP1-Phactr1 expression was induced by tetracycline as indicated. Phosphorylation of Phactr1/PP1 substrates IRSp53 S455 and Afadin S1275 is shown below.

C. Analysis of Phactr1/PP1 substrate Afadin pS1275 phosphorylation in Flp-In TRex 293 cells expressing PP1 and PP1-fusion proteins.

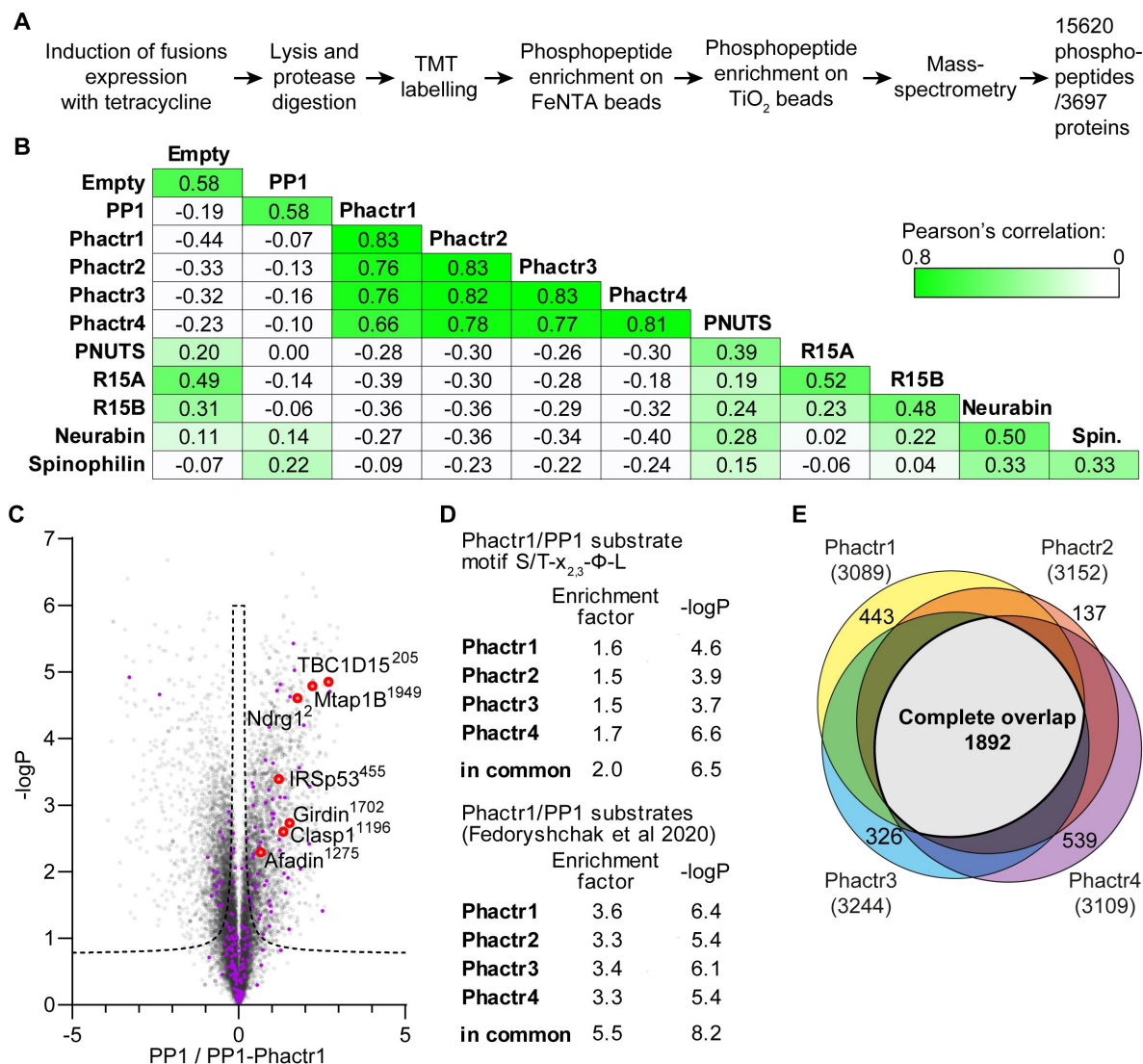


Figure 2.

PP1-PIP fusion phosphoproteomics.

A. TMT phosphoproteomics workflow.

B. Average sample-to-sample correlations between triplicates from cells expressing the different fusion proteins, PP1α(7-304)-SGSGS alone, or empty vector. For the same fusion-expressing cell lines, the average of Pearson coefficients of correlation within a triplicate are shown.

C. Phosphorylation sites enriched in PP1 samples as opposed to PP1-Phactr1 fusion samples. Purple - hits conforming to the Phactr1 substrate motif S/T-x_{2,3}-Φ-L. Red - top hits identified previously (Fedoryshchak et al., 2020). Dashed line, 5% false-discovery rate cutoff.

D. Enrichment of hits conforming to the Phactr1 substrate motif S/T-x_{2,3}-Φ-L and of hits identified in the previous study in all Phactr samples calculated using Fisher's exact test.

E. Venn diagram showing overlap between hits identified as potential Phactr1-4 substrates.

We next used the proteomics approach to investigate protein dephosphorylation by the PP1-R15A/B and PP1-PNUTS fusion proteins, comparing each fusion to all the others (other than its paralog) or PP1 α alone (**Figure 2B**). PPP1R15A has a well-validated substrate, eIF2 α pS51 (Novoa et al., 2001), whose effective dephosphorylation requires additional recruitment of G-actin to the PPP1R15A/PP1 complex (Chen et al., 2015; Yan et al., 2021). The eIF2 α pS51 phosphorylation site was not detected in the dataset, however, and no other phosphorylation sites were detectably depleted, apart from PPP6R1 S531, in cells expressing PPP1R15B (**Figure S3A,S3B**). Expression of the PP1-PNUTS fusion, which includes sequences that recruit WDR82 (Lee et al., 2010), led to specific depletion of phosphorylation sites from CXXC1/CFP1 and SET1B, which along with WDR82 are components of the COMPASS histone lysine *N*-methyl transferase complexes (Cenik and Shilatfard, 2021) (**Figure S3C**). These proteins bear no obvious sequence similarity in the vicinity of the dephosphorylation site (**Figure S3D**). These findings will be explored in future work.

New candidate substrates for Neurabin and Spinophilin

Having validated the PP1-PIP fusion approach, we focussed on Neurabin and Spinophilin, two PIPs implicated in neuronal plasticity (Sarrouilhe et al., 2006; Foley et al., 2021), which contain a PDZ domain implicated in recruitment of potential substrates (Burnett et al., 1998; Yan et al., 1999; Sarrouilhe et al., 2006; Kelker et al., 2007). The PDZ domain is separated from the RVxF- Φ -R-W string by a 5-turn α -helix, which remodels the PP1 hydrophobic groove in a manner distinct from Phactr1 (Ragusa et al., 2010; Fedoryshchak et al., 2020).

Expression of the PP1-Neurabin or PP1-Spinophilin fusions led to specific depletion of closely related sets of phosphorylation sites (**Figure 3A**, **3B**). These included multiple sites from the translational inhibitor proteins 4E-BP1 and 4E-BP2. Levels of total 4E-BP1 and 4E-BP2 proteins were not affected (Figures S3E). Phosphorylation sites from two other proteins, DTL and CAMSAP3, were also significantly depleted upon expression of both PP1-Spinophilin and PP1-Neurabin fusions, while a further 7 were specific to one fusion or the other. However, apart from a preference for proline at position +1, inspection these sequences did not reveal any obvious sequence similarities in the vicinity of the dephosphorylation site (**Figure 3C**). Substrates identified in the PP1-Phactr and PP1-PNUTS screens showed no detectable depletion, and *vice versa*, indicating that the substrates identified were specific for each fusion. Consistent with the phosphoproteomics data, immunoblotting analysis with phosphorylation-specific antibodies demonstrated that induction of PP1-Neurabin resulted in decreased phosphorylation of T70, S65/S101 and possibly T37/T46, while total 4E-BP1 resolved from a heterogeneous distribution to a largely monodisperse species (**Figure 3D**, **Figure S3F**).

The 4E-BPs are critical components of the mTORC1 growth control pathway which couples translation to nutrient availability and extracellular signals (reviewed by Hoeffler and Klann, 2010; Liu and Sabatini, 2020) (see Discussion). Phosphorylation of 4E-BPs potentiates translation by inhibiting their ability to sequester EIF4E (reviewed by Martineau et al., 2013; Romagnoli et al., 2021). Accordingly, expression of PP1-Neurabin, but not PP1 alone, suppressed translation in 293 cells (**Figure 3E**). These data establish the Neurabin/PP1 and Spinophilin/PP1 holoenzymes as potential negative regulators of the mTORC1 pathway (**Figure S3G**; see Discussion).

The PP1-Neurabin PDZ domain is required for 4E-BP1 dephosphorylation

To demonstrate a direct enzyme-substrate relationship between 4E-BP1 and PP1-Neurabin we expressed mCherry-tagged 4E-BP1 in 293 cells, recovered it on RFP-trap affinity beads, and incubated it with increasing amounts recombinant PP1-Neurabin. Analysis with the phospho-specific antibodies confirmed that pT37/46, pS65/101 and pT70 are all targets for dephosphorylation by PP1-Neurabin, with pT70 being somewhat preferred (**Figure 4A, 4B**).

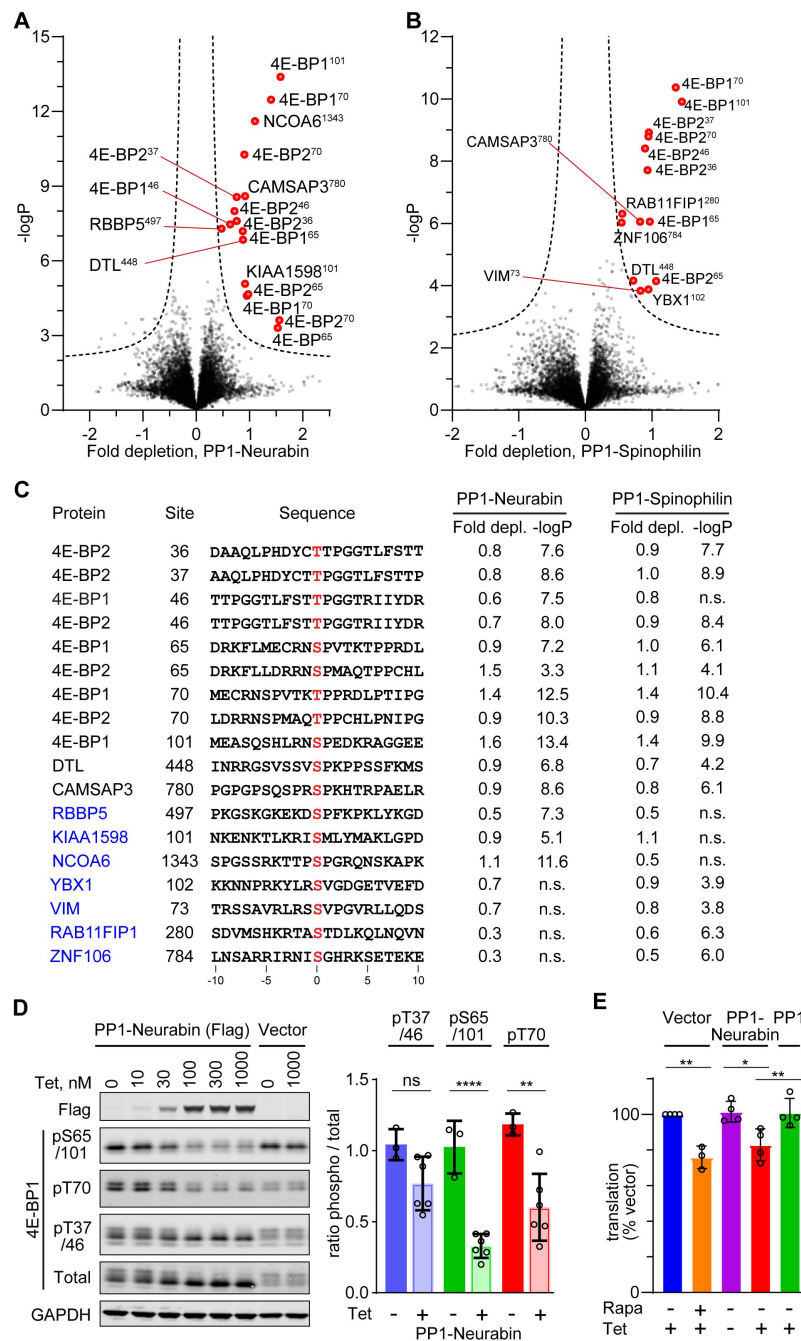


Figure 3.

Phosphoproteomics of PP1-Neurabin and PP1-Spinophilin.

A-B. Identification of PP1-Neurabin (**A**) and PP1-Spinophilin (**B**) substrates by depletion of phosphorylation sites in the corresponding samples compared to average abundance in the dataset (excluding PP1-Neurabin and PP1-Spinophilin). Dashed line, 5% false-discovery threshold; significantly depleted sites shown in red.

C. Sequences of significantly depleted phosphorylation sites identified in **A** and **B**.

D. Immunoblot analysis of 4E-BP1 phosphorylation sites in 293 Flp-In T-Rex cells upon expression of PP1-Neurabin or empty vector.

E. Protein synthesis quantification assay. 293 Flp-In T-Rex cells expressing vector alone, PP1-Neurabin, or PP1, were induced with tetracycline (50 nM) and/or treated with rapamycin (50 nM) for 16h as indicated before treatment with *O*-propargyl puromycin to label nascent polypeptides, which were conjugated to AlexaFluor-488 azide and quantified by flow cytometry. Fluorescence intensities were normalized to untreated cells.

Since the 4E-BP C-terminal sequences are similar to those of p70 S6K, previously shown to interact with the Neurabin PDZ domain (Burnett et al., 1998 [\[1\]](#)) (**Figure 4C** [\[1\]](#)), we considered the possibility that 4E-BP1 dephosphorylation at multiple sites reflects its recruitment through PDZ interaction.

Simple deletion of the 4E-BP1 C-terminal residues substantially blocked phosphorylation of transfected mCherry-4E-BP1 (**Figure S4A** [\[1\]](#)), reflecting the loss of the C-terminal TOR signalling (TOS) motif required for mTORC1 kinase recruitment and 4E-BP1 phosphorylation (Schalm and Blenis, 2002 [\[2\]](#); Yang et al, 2017 [\[3\]](#)). Since the C-terminal carboxylate, which is essential for PDZ interaction (Harris and Lim, 2001 [\[4\]](#); Subbaiah et al, 2011 [\[5\]](#)), is not part of the TOS motif, we generated mCherry-4E-BP1(118+A), in which an additional C-terminal alanine should still allow TOS-mediated phosphorylation, but prevent PDZ interaction. While mCherry-4E-BP1(118+A) was efficiently phosphorylated upon expression in 293 cells (**Figure S4A** [\[1\]](#)), its dephosphorylation *in vitro* required PP1-Neurabin concentrations some 20-50 times greater than the wildtype protein (**Figure 4A, 4B** [\[1\]](#)). These results suggest that the 4E-BP1 C-terminal sequences constitute a PDZ binding motif (PBM), and point to a role for the Neurabin and Spinophilin PDZ domains in substrate recognition.

We next used a fluorescence polarization assay to compare the PDZ-binding affinity of the 4E-BP C-terminal sequences with those of p70 S6K, and other proteins reported to be Neurabin/Spinophilin PDZ ligands (**Figure 4C** [\[1\]](#)) (Burnett et al., 1998 [\[1\]](#); Penzes et al, 2001 [\[6\]](#); Kelker et al., 2007 [\[7\]](#); Ragusa et al., 2010 [\[8\]](#)). The 4E-BP1 PBM, which is identical amongst all three 4E-BP isoforms, bound the PDZ domains with comparable affinities in the micromolar range, and binding was abolished by substitution of the C-terminal hydrophobic residues (**Figure 4C** [\[1\]](#), **4D** [\[1\]](#); **Figure S4B** [\[1\]](#)). These binding affinities were 10-30-fold greater than those p70 S6K and the RhoGEF Kalirin-7, which were of order 100 μ M, and >100-fold greater than various glutamate receptor C-terminal peptides (**Figure 4C** [\[1\]](#), **4D** [\[1\]](#); **Figure S4B** [\[1\]](#)). p70 S6K also functions in the mTORC1 pathway (for reviews see Liu and Sabatini, 2020 [\[9\]](#); Artemenko et al, 2022 [\[10\]](#)). Although most of its phosphorylation sites were not detected by phosphoproteomics, immunoblotting experiments demonstrated that PP1-neurabin expression decreased levels of the activating T389 phosphorylation (**Figure S4C** [\[1\]](#)).

PDZ domain interaction determines PP1-Neurabin specificity

We next compared how interactions with the PP1-Neurabin PDZ and the remodelled PP1 hydrophobic groove contribute to substrate specificity. To do this we compared the ability of PP1-Neurabin and PP1-Phactr1 to dephosphorylate synthetic peptides derived from their substrates 4E-BP1 and IRSp53. In these peptides 14^{mer} sequences spanning 4E-BP1 and IRSp53 dephosphorylation sites are joined via a GSG linker to the Neurabin C-terminal high affinity PDZ-binding motif of 4E-BP1, or its mutant derivative unable to bind the PDZ domain (**Figure 5A** [\[1\]](#)). The Neurabin substrate 4E-BP1^{WT} contains p4E-BP1 amino acids 64-78, including the phosphorylated T70 site, while the Phactr1 substrate IRSp53^{WT} contains IRSp53 residues 449-463, spanning the phosphorylated S455 site (**Figure 5A** [\[1\]](#), **Figure S5A** [\[1\]](#)).

PP1-Neurabin dephosphorylated 4E-BP1^{WT} with a catalytic efficiency some 100-fold greater than PP1 alone, while peptide 4E-BP1^{MUT}, which cannot bind the Neurabin PDZ domain, was 30-fold less reactive (**Figure 5B** [\[1\]](#), **Figure S5B** [\[1\]](#)). In contrast, PP1-Phactr1, dephosphorylated both 4E-BP1^{WT} and 4E-BP1^{MUT} at rates similar to those of PP1 alone (**Figure 5B** [\[1\]](#), **Figure S5B** [\[1\]](#)). The Neurabin sequences, specifically the PDZ domain, thus play a critical role in specific 4E-BP pT70 substrate recognition. PP1-Neurabin also dephosphorylated IRSp53^{WT} with a comparable catalytic efficiency, but this was entirely dependent on PDZ domain interaction, IRSp53^{MUT} being unreactive (**Figure 5B** [\[1\]](#), **Figure S5B** [\[1\]](#)). In contrast, both IRSp53^{WT} and IRSp53^{MUT} peptides were dephosphorylated by PP1-Phactr1 with a catalytic efficiency some 100-fold greater than PP1 alone. These results demonstrate the critical role played by the PDZ domain substrate specificity, and underscore the role played by PIPs in potentiating the catalytic efficiency of PIP/PP1 complexes.

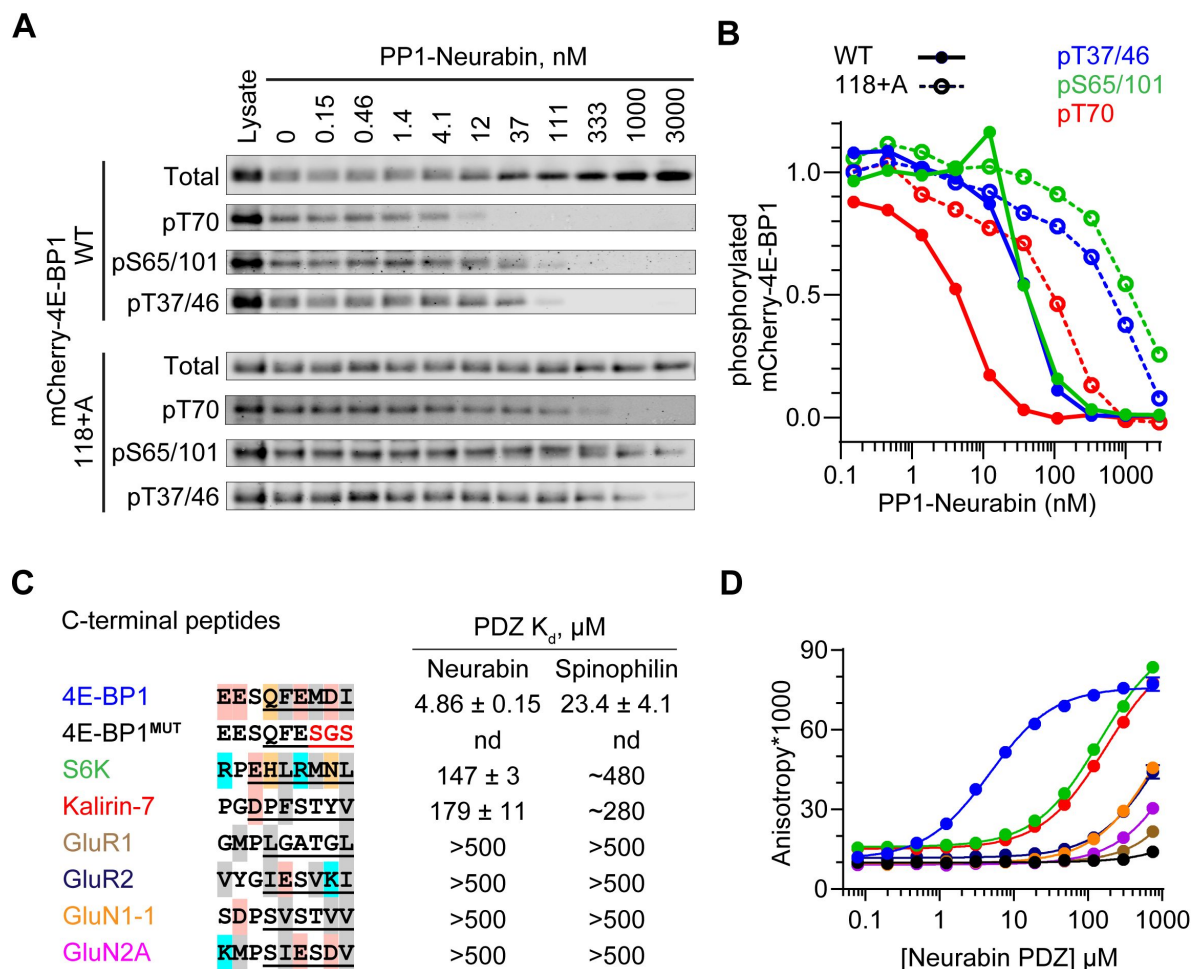


Figure 4.

4E-BP1 is a substrate of PP1-Neurabin.

A. mCherry-tagged wild-type 4E-BP1 or 4E-BP1(118+A) were expressed and purified from 293 cells, incubated with increasing amounts of recombinant PP1-Neurabin. Phosphorylation of the indicated sites was analysed by immunoblotting.

B. Quantification of **A**.

C. Left, sequence alignment of potential Neurabin/Spinophilin PDZ domain ligands.

Grey shading, hydrophobic residues; pink, acidic residues; cyan, basic residues; orange, hydrophilic residues. Underlining shows sequences N-terminally linked to 6-carboxyfluorescein (FAM) for use in fluorescence polarisation (FP) assay. Right, binding affinities for the Neurabin and Spinophilin PDZ domains as determined in the FP assay.

D. FP assay. FAM-labelled peptides (see **C**) were titrated with increasing concentrations of recombinant Neurabin PDZ domain and affinity estimated from change in fluorescence anisotropy. For Spinophilin data see [Figure S4B](#).

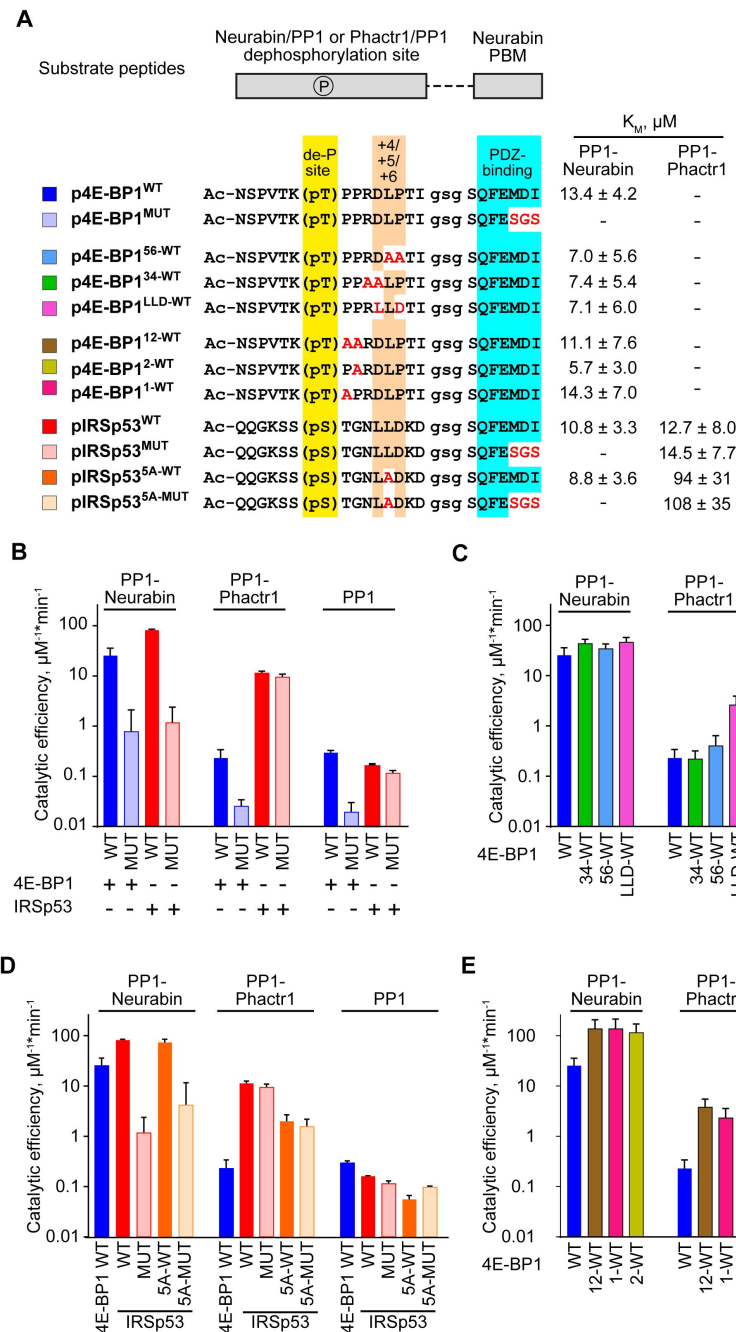


Figure 5.

Substrate specificity determinants of PP1-Neurabin.

A. Top, synthetic substrate peptides contain either the 4E-BP1 T70 or IRSp53 S455 phosphorylation sites, joined by a GSG linker to the Neurabin PDZ-binding C-terminal sequences. PBM, PDZ-binding motif. Below, sequences of the different peptides analysed; highlights indicate the dephosphorylation site (yellow), the +4/+6 region (orange), and the PDZ-binding sequence (cyan), with alanine and other substitutions indicated in red. Right, K_M and catalytic efficiencies; for catalytic efficiency quantification see [Figure S5A](#).

B-E. Peptides were treated with recombinant PP1-Neurabin, PP1-Phactr1 or PP1 in the presence of the phosphate sensor, and K_M and catalytic efficiencies determined. Panels show relative catalytic efficiencies as determined from data displayed in [Figure S5B-S5E](#). **B.** Comparison of Neurabin-PP1 and Phactr1-PP1 substrates 4E-BP1 and IRSp53. **C.** Role of the +4/+6 region in 4E-BP1 substrate recognition. **D.** Role of the +5 residue in IRSp53 substrate recognition. **E.** Role of 4E-BP1 +1/+2 residues.

Substrate interactions with the remodelled PP1 hydrophobic groove do not affect PP1-Neurabin specificity

We next assessed the potential role of the remodelled hydrophobic groove in substrate recognition. Positions +3 to +6 relative to the dephosphorylation site are critical for recognition of the remodelled hydrophobic groove by Phactr1/PP1 (Fedoryshchak et al., 2020 [DOI](#)), so we assessed the effect of mutations at these positions on catalytic activity. PP1-Neurabin dephosphorylated 4E-BP1^{WT} containing alanine substitutions, or IRSp53 sequences, at positions +3/4 or +5/6 with slightly increased catalytic efficiency (Figure 5C [DOI](#), Figure S5C [DOI](#)). These mutations had strikingly different effects on dephosphorylation by PP1-Phactr1. While the alanine substitutions had little effect, conversion of +4 to +6 to the IRSp53 sequence LLD increased catalytic efficiency some 20-fold (Figure 5C [DOI](#), Figure S5C [DOI](#)). Similar results were seen with the IRSp53 substrate peptides: alanine substitution in the groove-interacting region had no effect on PP1-Neurabin catalytic efficiency, but significantly impaired that of PP1-Phactr1 (Figure 5D [DOI](#), Figure S5D [DOI](#)). Strikingly, alanine substitutions at +1 and +2 in 4E-BP1^{WT} increased catalytic efficiency by both fusions, perhaps reflecting changes at the catalytic site itself (Figure 5E [DOI](#), Figure S5E [DOI](#)).

Taken together with the results in the preceding section, these data support a model in which PP1-Neurabin substrate specificity is driven predominantly by the ability of substrates to interact with its PDZ domain rather than the remodelled PP1 hydrophobic groove, in contrast to that of PP1-Phactr1, where the latter plays the dominant role (see Discussion).

Structural analysis of PP1/Neurabin – 4EBP-1 interaction

We next sought to visualise PP1-Neurabin/4E-BP1 interactions directly at the structural level. To do this, we used the “chimera” strategy previously used to examine Phactr1/PP1/substrate interactions, in which Phactr1 substrate sequences were fused C-terminally to PP1(7-304), and co-crystallised with the Phactr1 PP1-interacting C-terminal domain. This revealed a putative enzyme-product complex, with substrate sequences binding in a remodelled PP1 hydrophobic groove and serine and a presumed phosphate docked at the active site (Fedoryshchak et al., 2020 [DOI](#)).

Accordingly, we constructed an analogous PP1-4E-BP1 substrate fusion, comprising PP1(7-304) / (SG)₅ / 4E-BP1(65-83) / G / 4E-BP1(112-118) (Figure 6A [DOI](#)), co-expressed it with Neurabin residues 423-593, and determined the crystal structure of the purified complex at 2.36 Å resolution (Figure 6B [DOI](#); Table 1 [DOI](#)) (Ragusa et al., 2010 [DOI](#)).

In the complex, the PP1 catalytic core and Neurabin PDZ sequences were well resolved, along with the 4E-BP1 PBM, which was docked with the Neurabin PDZ domain (Figure 6B [DOI](#)). The individual domains were largely identical to a previously published structure of unliganded Spinophilin/PP1 (Ragusa et al., 2010 [DOI](#)) (PP1(1-304) RMSD 0.12 Å, PDZ(493-582) RMSD 0.45 Å). However, the PDZ domain in our Neurabin/PP1-4E-BP1 substrate complex structure is oriented at 21° to that in the unliganded Spinophilin/PP1 complex owing to a slight bend in the C-terminal section of the 5-turn α-helix that connects it to the RVxF-ΦΦ-R-W string (Figure 6C [DOI](#)). The 4E-BP1 PBM, 113(QFEMDI)118, uses a beta-strand addition mechanism to make extensive contacts with the Spinophilin PDZ domain similar to those seen in other PDZ-ligand complexes (see Harris and Lim, 2001 [DOI](#); Subbaiah et al., 2011 [DOI](#), for overview): 4E-BP1 F114, M116 and I118 make hydrophobic contacts with the Neurabin PDZ domain PBM-binding groove, while an extensive hydrogen bonding network is formed between 4E-BP1 F114, M116, and I118 main chain carbonyl and amide groups, and its C-terminal carboxylate, with main chain residues in the PDZ PBM-binding groove (L514, G515, I516, I518, and G520) (Figure 6D [DOI](#)).

Apart from the C-terminal sequences, the 4E-BP1 T70 substrate sequences were largely unresolved in the crystal structure. Unlike the Phactr1 substrate chimera, no interactions were seen with the remodelled PP1-Neurabin hydrophobic groove; and no virtual enzyme-product complex and solvent phosphate were detected at the active site, perhaps reflecting the absence of stabilising

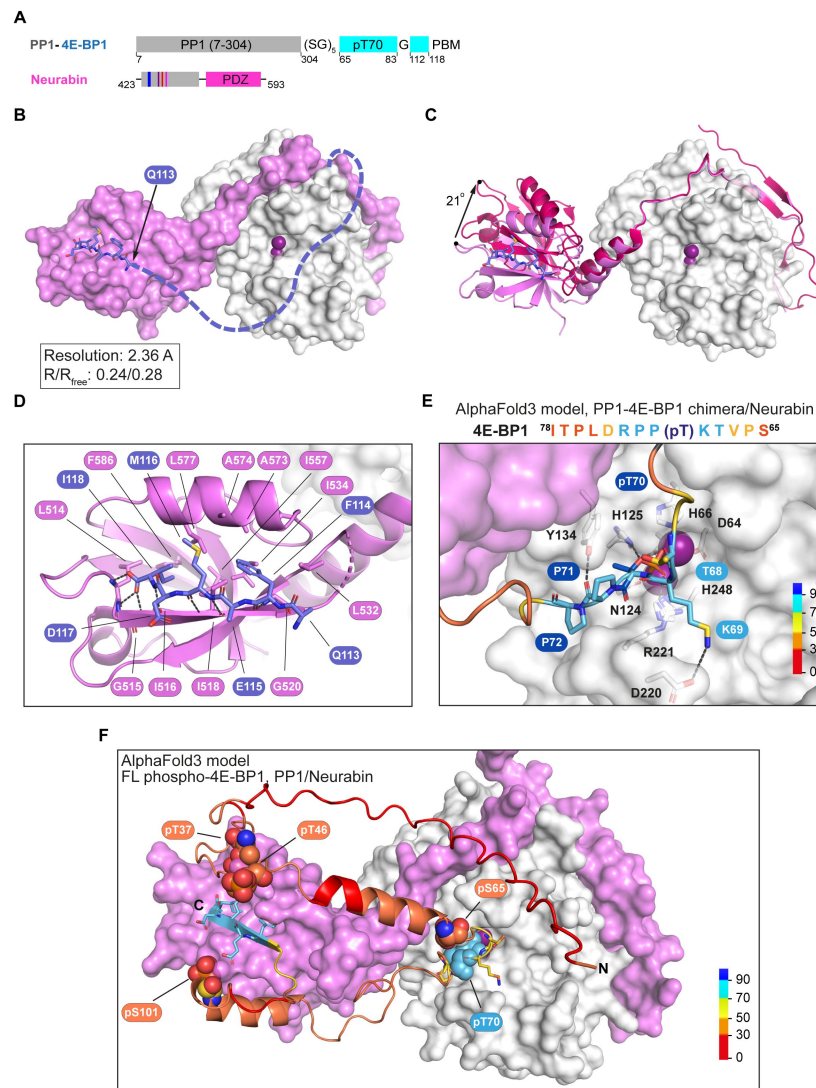


Figure 6.

Structural analysis of 4E-BP1 interactions with PP1-Neurabin.

- A.** Schematic of the PP1-4E-BP1 chimera and of Neurabin PP1-interacting and PDZ domain sequences.
- B.** Crystal structure of the PP1-4E-BP1/Neurabin complex. PP1 in white surface representation, Neurabin in lilac surface representation, 4E-BP1 in blue stick representation, with unresolved sequences indicated by dashed line. PP1 active site presumptive Mn^{2+} ions in purple.
- C.** Comparison of PP1-4E-BP1/Neurabin complex structure with previous Neurabin/PP1 holophosphatase structure (Ragusa et al., 2010). PP1 in white surface representation, Neurabin in ribbon representation (lilac, PP1-4E-BP1/Neurabin; red, Neurabin/PP1). 4E-BP1 in blue stick representation, unresolved sequences not shown. Structures are superimposed on PP1 residues 7-298 (rmsd=0.21 Å, 277 alpha carbons).
- D.** Close-up view of interactions between 4E-BP1 C-terminal sequences (blue sticks) with the Neurabin PDZ domain (lilac cartoons).
- E.** AlphaFold3 model of the phosphorylated PP1-4E-BP1 chimera / Neurabin(423-593) interaction. A close-up view of predicted interaction of pT70 with the PP1 catalytic site is shown. For PAE and pLDDT plots, see [Figure S6A](#). PP1 and Neurabin are shown respectively in white and lilac surface representation, with PP1 active site Mn^{2+} ions in purple. 4E-BP1 sequences are in stick representation, colour-coded according to the AlphaFold3 pLDDT score (inset). See also [Figure S6B](#), [S6C](#).
- F.** AlphaFold3 modelling of the Neurabin(423-593)/PP1 - 5x phospho-4E-BP1 interaction. PP1 and Neurabin are shown respectively in white and lilac surface representation, with PP1 active site Mn^{2+} ions in purple. 4E-BP1 sequences are in ribbon and stick representation, colour-coded according to the AlphaFold3 pLDDT score (inset), with the 4E-BP1 phosphorylations at T37, T46, S65, T70 and S101 shown in spheres. For PAE and pLDDT plots, see [Figure S6F](#).

| | (PDB accession number) |
|--------------------------------|-------------------------------|
| Resolution range | 52.48 - 2.36 (2.42 - 2.36) |
| Space group | C222 ₁ |
| Unit cell a, b, c | 104.95 130.64 156.13 |
| α , β , γ | 90 90 90 |
| Total reflections | 1 207 183 (85 193) |
| Unique reflections | 44 376 (3 023) |
| Multiplicity | 27.2 (28.2) |
| Completeness (%) | 98.91 (91.66) |
| Mean I/sigma(I) | 5.29 (0.20) |
| Wilson B-factor | 49.25 |
| R-merge | 0.31 (12.11) |
| R-meas | 0.32 (12.33) |
| R-pim | 0.06 (2.30) |
| CC1/2 | 0.99 (0.28) |
| Reflections used in refinement | 44 019 (2 889) |
| Reflections used for R-free | 1 996 (131) |
| R _{work} | 0.24 (0.36) |
| R _{free} | 0.28 (0.32) |
| Number of non-hydrogen atoms | 6 180 |
| macromolecules | 6 156 |
| ligands | 4 |
| solvent | 20 |
| Protein residues | 787 |
| RMS(bonds) | 0.003 |
| RMS(angles) | 0.61 |
| Ramachandran favoured (%) | 95.74 |
| Ramachandran allowed (%) | 4.26 |
| Ramachandran outliers (%) | 0.00 |
| Clash score | 3.23 |
| Average B-factor | 57.04 |
| macromolecules | 57.05 |
| ligands | 68.46 |
| solvent | 50.83 |

Table 1

Crystallographic data and refinement statistics.

hydrophobic groove interactions (**Figure 6B**). To gain insight into potential interactions at the PP1 catalytic site, we therefore used AlphaFold3 to model the PP1-4E-BP1 substrate chimera in its phosphorylated and unphosphorylated states (**Figure S6A, S6B**). While the 4E-BP1/ PDZ interaction was correctly predicted regardless of phosphorylation status, only the phosphorylated substrate was predicted to interact directly with the PP1 active site (**Figure 6E**, **Figure S6B, S6C**). The 4E-BP1 substrate sequence ⁶⁸TK(pT70)PPR⁷³, predicted with high confidence, docks at the catalytic site, with K69 interacting with D220^{PP1}, pT70 interacting with the metal ions, H125^{PP1} and R221^{PP1}, and P71 interacting with Y134^{PP1}, but the remodelled PP1 hydrophobic groove remains unoccupied (**Figure 6E**, **Figure S6B**). In contrast, AlphaFold3 gives only a low confidence prediction for the unphosphorylated substrate site D74 and L75 interacting with H125^{PP1}, and Y134^{PP1} (**Figure S6C, S6D**). These results are consistent with the biochemical studies, and support the notion that interaction with the remodelled hydrophobic groove plays no part in recognition of 4E-BP1 by the Neurabin/PP1 holoenzyme.

Finally we used AlphaFold3 to predict interactions between Neurabin/PP1 and full-length 4E-BP1 phosphorylated on T37, T46, S65, T70, or S101 (**Figure 6F**, **Figure S6F**). All the predictions placed the C-terminus of 4E-BP1 in the ligand-binding groove of the PDZ domain, docking the phosphorylated T70 site in the PP1 active site in a similar manner way to that seen in the substrate chimera predictions (**Figure 6F**; **Figure S6C**). Taken together with the crystallography and biochemical data, our observation support the view that the primary determinant of substrate specificity for Neurabin/PP1 is interaction with the PDZ domain adjacent to the RVxF-ΦΦ-R-W string.

Discussion

The PP1 catalytic subunit possesses little intrinsic sequence specificity. Instead it recognises specific substrates by forming holoenzymes in which it partners with a variety of PP1 interacting proteins (PIPs) to direct dephosphorylation to specific substrates. We previously showed that interaction of the Phactr1 PIP with PP1 remodels the PP1 hydrophobic substrate groove in such a way as to allowing specific recognition of substrate sequences C-terminal to the dephosphorylation site (Fedoryshchak et al., 2020). Phactr1 belongs to a group of PIPs that recognise PP1 using a common RVxF-ΦΦ-R-W string, all of which potentially remodel the hydrophobic groove; indeed, structural studies confirm that Spinophilin does this differently from the Phactrs (Ragusa et al., 2010; Fedoryshchak et al., 2020). We identified potential substrates for the other RVxF-ΦΦ-R-W PIPs, and elucidate mechanisms of substrate recognition, focussing on the Neurabin and Spinophilin PIPs.

Our previous study showed that a fusion protein comprising PP1 joined to Phactr1 sequences C-terminal to the RVxF motif maintains both the structure and the sequence-specificity of the intact Phactr1/PP1 holoenzyme (Fedoryshchak et al., 2020). We used this fusion approach, in conjunction with MS phosphoproteomics in 293 cells, to compare the specificities of the different Phactr family members, and to identify potential substrates for other RVxF-ΦΦ-R-W PIPs. All four PP1-Phactr fusions exhibited virtually identical substrate specificities, which were substantially similar to that of the authentic Phactr1/PP1 holoenzyme, giving confidence that findings made with the fusions are also applicable to other RVxF-ΦΦ-R-W PIP/PP1 holoenzymes. It is likely that differential intracellular targeting and/or tissue-specific expression of the four different Phactr/PP1 holoenzymes allows further refinement of substrate specificity.

Expression of the other PP1-(RVxF-ΦΦ-R-W PIP) fusions revealed potential substrates for PNUTS and PP1-Neurabin/Spinophilin, but not PP1-PPP1R15A/B. Unlike the PP1-Phactr substrates, however, these exhibited no obvious sequence similarities in the substrate sequences adjacent to the targeted dephosphorylation remodelled hydrophobic groove. For PNUTS, we identified only the SET1A/B-COMPASS complex components CXXC1/CFP1 and SETD1B (Cenik and Shilatifard,

2021 [\[1\]](#)). These may be recruited to PNUTS by interaction with its binding partner WDR82, which is also present in SET1A/B-COMPASS complexes (Cenik and Shilatifard, 2021 [\[2\]](#)), but further work will be necessary to confirm this.

Expression of the PP1-Neurabin and PP1-Spinophilin fusions identified nine potential substrates with eighteen candidate dephosphorylation sites, of which eight represented conserved mTORC1 dependent phosphorylations of the translational regulators 4E-BP1 and 4E-BP2. Using immunoblotting we found that the p70 S6K activating phosphorylation at T389 also appears to be a substrate for PP1-Neurabin. The 4E-BPs and p70 S6K are critical targets of the mTORC1 pathway, which links translational control to cell nutrient status and extracellular signals in multiple settings (Hoeffler and Klann, 2010 [\[3\]](#); Liu and Sabatini, 2020 [\[4\]](#)). Consistent with this, we found that overexpression of PP1-Neurabin can suppress translation when expressed in 293 cells. It therefore is likely that Neurabin and Spinophilin can negatively regulate both arms of the mTORC1 protein synthesis pathway (Figure S3G [\[5\]](#)).

The presence of multiple dephosphorylation sites on the 4E-BPs with no obvious primary sequence homology raised the question of how these targets are recognised. We found that dephosphorylation of 4E-BP1 by PP1-Neurabin requires its C-terminal sequences, which constitute a PDZ-binding motif (PBM). The micromolar affinity of this interaction, which is stronger than that previously reported for p70 S6K (Burnett et al., 1998 [\[6\]](#)), may reflect the necessity for effective competition with the mTORC1 kinase complex, which binds the 4E-BPs using a C-terminal TOS motif that overlaps the PBM (Schalm and Blenis, 2002 [\[7\]](#); Yang et al., 2017 [\[8\]](#)). In contrast, we found that other reported ligands, such as the glutamatergic and dopaminergic receptors (Kelker et al., 2007 [\[9\]](#)) bind the Neurabin/Spinophilin PDZ domains with much lower affinity. In neurons, association of these receptors with Neurabin and PP1 correlates with channel activity and dephosphorylation (Wu et al., 2008 [\[10\]](#); Yan, 1999 #29, reviewed by Foley et al., 2021 [\[11\]](#)). It remains possible that Neurabin/Spinophilin oligomerisation and/or F-actin binding, and receptor membrane localisation, effectively increases the avidity of such weak PBM-PDZ interactions, but more work is required to establish whether these channels are direct Neurabin/PP1 substrates.

We used synthetic peptide substrates derived from 4E-BP1, or the Phactr1/PP1 substrate IRSp53, to investigate how the substrate recognition mechanisms differ between the PP1-Neurabin and PP1-Phactr fusions. In the context of the PP1-PIP fusions, and by extension in that of the PIP/PP1 holoenzyme, the PIP sequences play a critical role in directing substrate specificity and potentiating catalytic efficiency. In the PP1-Neurabin fusion, interaction with the PDZ domain is the critical determinant of both catalytic efficiency and specificity: it increases catalytic efficiency 100-fold above that seen with PP1 alone, or the PP1-Phactr1 fusion. Moreover, the PP1-Neurabin fusion was inactive with the Phactr1/PP1 substrate IRSp53 unless the latter was made competent to bind the Neurabin PDZ domain. Our observations suggest a model in which 4E-BPs are recruited to Neurabin/PP1 via high affinity PBM-PDZ interaction, with the relatively low affinity of active-site interaction allowing dephosphorylation of the multiple sites during one round of PDZ binding. In contrast, dephosphorylation of the Phactr1/PP1 target IRSp53 pS455 by the PP1-Phactr1 fusion protein was critically dependent on interaction with the remodelled hydrophobic groove, consistent with our previous data (Fedoryshchak et al., 2020 [\[12\]](#)).

Several lines of evidence support the view that interaction with the remodelled PP1 hydrophobic groove plays no role in PP1-Neurabin substrate recognition. First, the PP1-Neurabin substrates we identified have obvious sequence similarity at positions +3 to +6, the sequences that potentially interact with the remodelled hydrophobic groove, and alanine substitutions at these positions do not influence PP1-Neurabin catalytic activity. Structural analysis of a PP1-4E-BP1 substrate fusion complexed with Spinophilin, also revealed no substrate contacts with PP1, although the PDZ-4E-BP1 interaction was well-resolved. Finally AlphaFold modelling of complexes formed between 4E-

BP1 substrates and the Spinophilin/PP1 holoenzyme predicted phosphorylation-specific interactions with the PP1 catalytic site, but no interactions with the remodelled hydrophobic groove.

Although the remodelled hydrophobic groove does not play a role in 4E-BP recognition by Neurabin/PP1, this does not necessarily mean that sequence-specific dephosphorylation by other PIP/PP1 complexes and substrate recruitment by protein interactions are inherently mutually exclusive: in principle a PIP could recruit substrates through protein interactions, and remodel the PP1 substrate binding grooves to allow discrimination between different phosphorylated sites on the target protein. That said, we think it likely that the other RVxF-ΦΦ-R-W PIPs will also recruit substrates by interaction with other PIP domains, or proteins bound to them. Such interactions might involve WDR82 for PNUTS, and G-actin for PPP1R15A/B (Yan et al., 2021 [↗](#); Erickson et al., 2024 [↗](#)).

Our findings establish Neurabin/PP1 and Spinophilin/PP1 holoenzymes as new candidate regulators of the mTORC1 pathway. Many studies have focussed on mTORC1 regulation of translation on the control of cell growth, particularly in cancer settings (Liu and Sabatini, 2020 [↗](#)), and previous work has shown that endogenous PP2C ψ /PPM1G contributes to 4E-BP1 dephosphorylation in 293 and HCT116 cells (Liu et al., 2013 [↗](#)). Localised translational regulation is also important in other settings, however, including neuronal development and function (Holt et al., 2019 [↗](#)). Here, mTORC1 signalling plays an important role in neuronal plasticity (Hoeffer and Klann, 2010 [↗](#)), as do both Neurabin and Spinophilin, which are largely neuron specific and enriched in dendritic spines (Wu, 2008 #75, reviewed by Foley et al., 2021 [↗](#)), and the 4E-BPs, particularly 4E-BP2 (for references see Aguilar-Valles et al., 2015 [↗](#)). Our finding that 4E-BPs are Neurabin/PP1 substrates potentially establishes a direct link between Neurabin and neuronal mTORC1 signalling (**Figure S3G** [↗](#)), which will be an interesting topic for future investigation.

Methods

Plasmids

NEBuilder HiFi DNA Assembly Cloning Kit and NEB Q5® Site-Directed Mutagenesis Kit were used according to manufacturer's protocols for plasmid assembly and mutagenesis. All primers are listed in Supplementary Table 1.

PIP sequences were amplified from 293 cells cDNA, except for the Neurabin sequence which was commercially synthesized. pET28-PP1(7-300) and pET28-PP1(7-304)-SGSGS-Phactr1(526-580) Phactr1 plasmids were as described (Fedoryshchak et al., 2020 [↗](#)). Other fusion proteins were expressed pET28-based expression plasmids were used to express other PP1-PIP fusions as follows: PP1(7-304)-SGSGS-Phactr2(580-634); PP1(7-304)-SGSGS-Phactr3(505-559); PP1(7-304)-SGSGS-Phactr4(648-702); PP1(7-304)-SGSGS-Neurabin(464-610); PP1(7-304)-SGSGS-Spinophilin(456-602); PP1(7-304)-SGSGS-R15A(562-674); PP1(7-304)-SGSGS-R15B(647-713); PP1(7-304)-SGSGS-PNUTS(408-619).

For T-Rex cell lines, pOG44 (Thermo) and pcDNA5/FRT/TO plasmids (Thermo) were used in conjunction with N-terminally Flag-tagged PP1-PIP fusions were inserted into pcDNA5/FRT/TO.

pcDNA3.1 IRSp53 and pcDNA3.1 IRSp53 L460A were as described (Fedoryshchak et al., 2020 [↗](#)). To obtain pEF-mCherry-4E-BP1, the 4E-BP1 sequences were amplified from 293 cells and inserted into pEF-mCherry plasmid. Site-directed mutagenesis was used to derive mutants Δ PDZ, 118+A, S65A, S101A, S65A/S101A. pGEX-Neurabin(PDZ) and pGEX-Spinophilin(PDZ) plasmids were obtained by cloning Neurabin and Spinophilin PDZ domains into the pGEX 6P2 vector (GE Healthcare). The PP1-4E-BP1 chimera was generated by insertion of 4E-BP1 sequences into pET28-PP1.

Cell lines and transfections

Commercially available 293 Flp-In T-REx cells and pOG44 + pcDNA5/FRT/TO stably transfected derivatives were used throughout. Cells were maintained in a humidified incubator at 37°C and 5% CO₂ and cultured in DMEM (Gibco) supplemented with 10% FCS (Gibco) and penicillin-streptomycin (Sigma). Prior to stable transfection, 293 Flp-In T-REx cells were maintained with 100 mg/mL Zeocin (Invivogen). Stably transfected 293 Flp-In T-REx derivative cell lines were cultured in a medium supplemented with 5 mg/mL Blasticidin (Invivogen) and 100 mg/mL Hygromycin B (Invivogen).

For stable transfection of a PP1-fusion protein, pOG44 and pcDNA5/FRT/TO-PP1-fusion plasmids were mixed at a ratio of 9:1. Lipofectamine™ 2000 (Invitrogen) in Opti-MEM® (Gibco) was added and transfection was done following the manufacturer's protocol. 100 mg/mL Hygromycin B (Invitrogen) was added to start the selection of stable cell line 2 days after transfection. Selection was complete and cell line stocks were frozen after 14 days.

pEF IRSp53 and pEF-mCherry-4E-BP1 plasmids were transfected with Lipofectamine™ 2000 (Invitrogen) in Opti-MEM® (Gibco) following the manufacturer's protocol. Cells were lysed 1 day after transfection in a buffer containing 20 mM Tris pH 7.4, 150 mM NaCl, 1 mM EDTA, 1 mM EGTA, 1% Triton X-100, 10% glycerol, 0.2% SDS. Lysates were cleared by centrifugation. 4x LDS sample buffer supplemented with DTT was added before running Immunoblots. Unless otherwise indicated, 1000 nM of tetracycline was used to express the PP1 fusion proteins in stably transfected 293 Flp-In T-REx cells, and the experiments were performed 16 h post-induction.

Immunoblotting

SDS-PAGE analysis of cell lysates and immunoblotting was performed using standard techniques; the signal was visualised and quantified using Odyssey CLx instrument (LI-COR) and the Image Studio (LI-COR) Odyssey Analysis Software. Primary antibodies used were Flag (1:2000, clone M2, Sigma F7425, mouse), IRSp53 (1:1000, Abcam ab15697), IRSp53 pS455 (1:500, previously described in Fedoryshchak 2020), Afadin (1:200, Santa Cruz sc-74433), Afadin pS1275 (1:500, previously described in Fedoryshchak 2020), Gapdh (1:2000, clone 0411, Santa Cruz sc-47724), 4E-BP1 (1:1000, Cell Signalling 9452), 4E-BP1 pT37/46 (1:1000, Cell Signalling 9459), 4E-BP1 pS65 (1:1000, Cell Signalling 9451), 4E-BP1 pT70 (1:1000, Cell Signalling 9455), mCherry (1:1000, clone 16D7, Thermo M11240, rat), S6K (1:1000, Cell Signalling 9202), S6K pS371 (1:1000, Cell Signalling 9208), S6K pT389 (1:1000, Cell Signalling 9205), S6K pT421/pS424 (1:1000, Cell Signalling 9204). Secondary antibodies labelled with IRDye 800CW and IRDye 680LT were from LI-COR.

Proteomics

Total and phospho-proteomics experiment was performed according to a detailed protocol previously published (Jones et al, 2020 [DOI](#)). Cells expressing PP1-PIP fusion proteins, PP1 only, or vector alone were induced with tetracycline for 16h. Cells were lysed in buffer containing 8 M Urea, 50 mM HEPES pH 8.5, 10 mM Glycerol 2-phosphate, 50 mM NaF, 5 mM Sodium pyrophosphate, 1 mM EDTA, 1 mM Sodium vanadate, 1 mM dithiothreitol, 1:50 protease inhibitor cocktail (Roche), 1:100 Phosphatase inhibitor cocktail, 400 nM Okadaic acid. Cysteines were reduced and alkylated by iodoacetamide followed by trypsin/rLysC protease digestion. Peptide samples were labelled with 10-plex (UK288606) and additionally 131C (VC294053) TMT reagents from Thermo and pooled. Part of the sample was injected saved for the total proteome analysis. The rest of the sample was used for 2-step phosphopeptide enrichment on TiO₂ beads (Thermo) and FeNTA beads (Thermo). Phosphopeptides were fractionated. Total proteome and enriched phosphopeptide fractions were separated on a 50 cm, 75 µm I.D. Pepmap column over a 2 h

gradient and eluted directly into the Orbitrap Fusion Lumos, operated with Xcalibur software, with measurement in MS2 and MS3 modes. The instrument was set up in data-dependent acquisition mode, with top 10 most abundant peptides selected for MS/MS by HCD fragmentation.

Raw mass spectrometric data were processed in MaxQuant (version 1.6.12.0); database search against the *Homo sapiens* canonical sequences from UniProtKB was performed using the Andromeda search engine. Fixed modifications were set as Carbamidomethyl (C) and variable modifications set as Oxidation (M), Acetyl (Protein N-term) and Phospho (STY). The estimated false discovery rate was set to 1% at the peptide, protein, and site levels, with a maximum of two missed cleavages allowed. Reporter ion MS2 or Reporter ion MS3 was appropriately selected for each raw file.

Phosphorylation site tables were imported into Perseus (v1.6.14.0) for analysis. Contaminants and reverse peptides were cleaned up from the Phosphosites (STY) and the values normalised and averaged between MS2 and MS3 datasets using Z-score function across columns. All samples were analysed as triplicates, except PP1-Spinophilin and PP1-PNUTS, for which duplicates were used due to the presence of an outlier dataset as determined by principal component analysis. Phosphorylation site enrichments were compared using multiple t-test with permutation based false-discovery cutoff at 5% unless indicated otherwise. Enrichment data are summarised in Table S2.

Mass spectrometry proteomics data have been deposited to the ProteomeXchange Consortium via the PRIDE partner repository with the dataset identifier PXD055166.

Peptides

Peptides were synthesized by the Francis Crick Institute Chemical Biology Science Technology Platform using standard Fmoc-SPPS techniques.

| Name | Sequence (FAM, 6-Carboxyfluorescein; eahx, aminohexanoic acid linker; OH, carboxyl at C-terminus) |
|--------------------------|---|
| 4EBP | FAM-eahx-QFEMDI-OH |
| 4EBP-mut | FAM-eahx-QFESGS-OH |
| S6K | FAM-eahx-EHLRMNL-OH |
| Kalirin-7 | FAM-eahx-DPFSTYV-OH |
| GluR1 | FAM-eahx-LGATGL-OH |
| GluR2 | FAM-eahx-IESVKI-OH |
| GluN1-1 | FAM-eahx-SVSTVV-OH |
| GluN2A | FAM-eahx-SIESDV-OH |
| | |
| 4E-BP1 ^{WT} | Ac-NSPVTK (pT) PPRDLPTIGSGSQFESGS-OH |
| 4E-BP1 ^{LLD-WT} | Ac-NSPVTK (pT) PPRLLDTIGSGSQFEMDI-OH |
| IRSp53 ^{WT} | Ac-QQ GKSS (pS) TGNLLDKDGSQFEMDI-OH |
| IRSp53 ^{MUT} | Ac-QQ GKSS (pS) TGNLLDKDGSQFESGS-OH |
| IRSp53 ^{5A-WT} | Ac-QQ GKSS (pS) TGNLADKDGSGSQFEMDI-OH |
| IRSp53 ^{5A-MUT} | Ac-QQ GKSS (pS) TGNLADKDGSGSQFESGS-OH |
| 4E-BP1 ^{12A-WT} | Ac-NSPVTK (pT) AARDLPTIGSGSQFEMDI-OH |
| | |
| 4E-BP1 ^{34A-WT} | Ac-NSPVTK (pT) PPAALPTIGSGSQFEMDI-OH |
| 4E-BP1 ^{56A-WT} | Ac-NSPVTK (pT) PPRDAATIGSGSQFEMDI-OH |
| 4E-BP1 ^{1A-WT} | Ac-NSPVTK (pT) APRDLPTIGSGSQFEMDI-OH |
| 4E-BP1 ^{2A-WT} | Ac-NSPVTK (pT) PARDLPTIGSGSQFEMDI-OH |

Protein expression and purification

PP1-fusion proteins were produced as 6xHis-tagged fusion proteins in (DE3) *E. coli* cells (Invitrogen) with pGRO7 co-expression as described (Choy et al., 2014). Overnight pre-cultures (400ml) were grown in LB medium supplemented 1 mM MnCl₂ and used to inoculate a 100L fermenter. After growth to OD₆₀₀ of ~0.5, 2 g/L of arabinose was added to induce GroEL/GroES expression. At OD₆₀₀ ~1, the temperature was lowered to 17°C and protein expression induced with 0.1 mM IPTG for ~18 hours. Cells were harvested, re-suspended in fresh LB medium/1mM MnCl₂/200 µg/ml chloramphenicol and agitated for 2h at 17°C. Harvested cells were resuspended in lysis buffer (50 mM Tris-HCl, pH 8.5, 5 mM imidazole, 700 mM NaCl, 1mM MnCl₂, 0.1% v/v TX-100, 0.5 mM TCEP, 0.5 mM AEBSF, 15 µg/ml benzamidine and complete EDTA-free protease inhibitor tablets), lysed by French press, clarified, and stored at -80°C.

Clarified lysates were loaded onto a 5ml HisTrap crude column on an AktaPure HPLC, washed with 20CV of buffer A (25 mM Tris-HCl pH 8.5, 250 mM NaCl, 10mM imidazole pH 8, 1mM MnCl₂), His-tagged fusion proteins were eluted in buffer B (Buffer A + 240mM Imidazole) and purified using size exclusion chromatography on a Superdex 200 26/60 column in SEC buffer1 (25 mM Tris-HCl pH 8.5, 200 mM NaCl, 0.5mM TCEP, 10 mM imidazole). The His tag was then cleaved off by incubating overnight with His-Tev protease at 4°C and the cleaved product recovered by passage of the sample over a 5ml HisTrap crude column. Protein was then concentrated and further purified on a Superdex 75 equilibrated in SEC buffer2 (25 mM Tris-HCl pH 8.5, 200 mM NaCl, 0.5mM TCEP). The PP1-Fusion proteins were concentrated to 10 mg/ml and stored at -80°C.

His-tagged Neurabin and Spinophilin PDZ domains were produced in BL21 (DE3) *E. coli* cells (Invitrogen). Overnight pre-cultures were grown in LB medium, 15 ml was used to inoculate 1L of TB media in a 2L baffled flasks. When OD₆₀₀ =1, the temperature was lowered to 20°C and protein expression induced by addition of 0.1 mM IPTG for ~18 hours. Harvested cells were resuspended in lysis buffer (50 mM Tris-HCl, pH 8.5, 5 mM imidazole, 700 mM NaCl, 0.1% v/v TX-100, 0.5 mM TCEP, 0.5 mM AEBSF, 15 µg/ml benzamidine and complete EDTA-free protease inhibitor tablets), lysed by French press, clarified, and stored at -80°C. PDZ domains were purified using the same protocol as PP1-fusion proteins without addition of 1mM MnCl₂ in the buffers.

Crystallisation and structure determination

PP1-4E-BP1/Neurabin was concentrated to 10 mg/ml and crystallised at 20°C using sitting-drop vapour diffusion. Sitting drops of 1 µl consisted of a 1:1 (vol:vol) mixture of protein and well solution (20% PEG 6000, 0.2M MgCl₂, 0.1 M MES pH 6.0). Crystals appeared within 5 days and reached maximum size after 7 days. Crystals were cryoprotected in well solution supplemented with 15% Glycerol + 15% ethylene glycol and flash-frozen in liquid nitrogen. 100 K at beamlines I04 (mx25587-44) of the Diamond Light Source Synchrotron (Oxford, UK). Data collection and refinement statistics are summarized in **Table 1**. Data sets were indexed, scaled and merged with xia2 (Winter et al., 2013). Molecular replacement used the atomic coordinates of human PP1 from PDB 4M0V (Choy et al., 2014) in PHASER (McCoy et al., 2007). Refinement used Phenix (Adams et al., 2010). Model building used COOT (Emsley et al., 2010) with validation by PROCHECK (Vaguine et al., 1999). Two copies of the complex were modelled in the asymmetric unit, but the entire PDZ domain of one copy was poorly defined in the density and therefore not modelled. The same issue was previously observed for the unliganded Spinophilin/PP1 structure (Ragusa et al., 2010). For structure analysis we used the second copy of the complex showing well-resolved density for PP1-4E-BP1 chimera and Neurabin. AlphaFold3 predictions (Abramson et al., 2024) were performed using the AlphaFold3 server. Output structure prediction and parameter files are presented in Supplementary Data File 1.

Fluorescence polarisation assay

FAM-labelled peptides were dissolved in a buffer 25 mM Tris-HCl pH 8, 250 mM NaCl, 0.5 mM TCEP. Peptide concentration was measured using Thermo Scientific NanoDrop One by FAM fluorescence at 495 nm. FP assays (10 µl final volume) were performed in 384-well plates. 2 µl of 500 nM peptide solutions were added to each well (100 nM final concentration). 8 µl of Neurabin PDZ or Spinophilin PDZ was added as a serial dilution, starting at 1000 µM (800 µM final concentration). Anisotropies were read out on BMG Labtech CLARIOstar Plus microplate reader. Binding constants were estimated in GraphPad Prism 8 by fitting readouts with the following equation:

$$A = A_f + (A_b - A_f) * (K_d + L + C - \frac{(K_d + L + C)^{0.5}}{2 * L})$$

(A, anisotropy measured; A_f , anisotropy of free peptide; A_b , anisotropy of bound peptide; L, labelled peptide concentration; C, Protein concentration (X axis); K_d , binding constant).

Phosphatase activity assays

Phosphopeptides were dissolved in 25 mM Tris-HCl pH 8, 250 mM NaCl buffer. Peptide concentration was measured using DeNovix DS-11 based on absorbance values at 215 nm. Assays (10 µl final volume) were performed in 384-well plates. The activity of the PP1 fusion preparation was established on the day of each experiment, using 50 µM pIRSp53^{WT} peptide as standard, with PP1-Phactr1 and PP1-Neurabin at various dilutions.

Peptides (4 µl) were serially diluted 2-fold from 1mM in complex buffer (1 mM MnCl₂, 25 mM Tris-HCl pH 8, 250 mM NaCl, 0.5 mM TCEP). 2 µl of 5x Phosphate sensor (Thermo) was added to the wells. 2 µl of PP1-fusion protein was added to the wells and fluorescence measurements were started immediately and taken every 3 min or 5 min using BMG Labtech CLARIOstar Plus microplate reader. Data was collected for 15 min at room temperature. Phosphate standards were measured to convert fluorescence readouts into phosphate concentration using a standard curve. Difference in fluorescence between the last and first data point was used as a readout.

A concentration of PP1-Phactr1 and PP1-Neurabin was chosen such that readouts were in the linear range of the Phosphate sensor detection. To measure K_M and catalytic efficiency (CE), an assay with varying dilutions of phosphopeptides was set up. 4 µl of a corresponding peptide dilution was added to wells, followed by 2 µl of 5x Phosphate sensor. 2 µl of PP1-fusion protein was added to the wells and fluorescence measurements were started immediately and taken every 3 min (alternatively, every 5 min). Data was collected for 15 min at room temperature.

Phosphate standards were measured to convert fluorescence readouts into phosphate concentration using a standard curve. Difference in fluorescence between the last and first data point was used as a readout. Rate constants were estimated in GraphPad Prism 8 by fitting readouts to modified Michaelis-Menten equation:

$$\frac{P}{t * E} = \frac{[k_{cat}]}{[K_M]} * \frac{C}{(K_M + 1)}$$

(P, phosphate released per time t; E, PP1-fusion concentration; $[k_{cat}/K_M]$, catalytic efficiency; C, initial phosphopeptide concentration; K_M , Michaelis constant).

4E-BP1 dephosphorylation immunoblot assay

293 Flp-In T-REx cells were transfected with mCherry-4E-BP1 (WT or 118+A mutant). Cells were lysed on the following day in the Tris-Triton buffer (see above). mCherry tagged constructs were enriched from the lysates using RFP-trap magnetic agarose beads (ChromoTek, rtma-20) using

manufacturer's protocol. Enriched fractions were eluted from the beads with 500 μ l 200 mM glycine pH 2.5, resulting in pure phosphorylated solution of mCherry-4E-BP1 (WT or 118+A mutant). Serial dilutions of PP1-Neurabin (0-1000 nM final concentration) were added to 40 μ l aliquots of mCherry-4E-BP1 (WT or 118+A mutant) 8 μ l and incubated for 15 min at room temperature before addition of 18 μ l 4x LDS sample buffer with DTT. The samples were warmed to 70°C for 10min before analysis by immunoblotting.

Protein synthesis assay

293 Flp-In T-Rex cells were culture in a 6-well plate. PP1, PP1-Neurabin or vector construct expression were induced 16 h before the experiment with 1 μ M tetracycline. Rapamycin was used at 50 nM for 16 h. *O*-propargyl puromycin (OPP; 5 μ M) was added to the culture for 30 min. Then cells were washed once with PBS and resuspended using trypsin. Cells were collected by centrifugation at 300g for 5 min, then washed once with PBS and 4% PFA was added for 15 min. Cells were collected and resuspended in 0.5% Triton-X100 in PBS for 15 min. Cells were collected and resuspend in 2% BSA in PBS twice. Click-reaction mixture was prepared as follows: 1540 μ L of water, 200 μ L of 10x PBS, 40 μ L CuSO₄ (20mM) and BTAA (100mM) mixture, 20 μ L of 5 mM AlexaFluor-488 azide, 200 μ L 100 mM sodium ascorbate.

200 μ L of click-reaction mixture was added to each sample and incubated for 30 min in the dark. Cells were collected and resuspended in 10 mM EDTA. Then cells were incubated for 30 min in H33342 1:10000 in PBS. Cells were washed with PBS and analysed on BD LSRFortessa Cell Analyzer. FlowJo software was used to analyse flow cytometry data. Single cells readouts were isolated using forward and side scatter parameters. Mean fluorescent intensity in AlexaFluor-488 channel was used as assay readout.

Acknowledgements

We thank Sila Ultanir for helpful discussions, insights into neuronal plasticity, and support for pilot experiments in neurons, and lab members, Neil McDonald, and Sila Ultanir for helpful discussions and comments on the manuscript. We thank Helen Flynn from Crick Proteomics STP for assistance with phosphoproteomics experiments, Jo Redmond from Chemical Biology STP for help discussions about substrate specificity assistance with peptide synthesis, and Simone Kunzelman from the Structural Biology STP for assistance with FP assay. This work was supported by the Francis Crick Institute which receives its core funding from Cancer Research UK (CC2102), the UK Medical Research Council (CC2102), and the Wellcome Trust (CC2102). This research was funded in whole, or in part, by the Wellcome Trust CC2102. For the purpose of Open Access, the author has applied a CC BY public copyright licence to any Author Accepted Manuscript version arising from this submission. The authors have no conflicts of interest.

Author contributions

ROF designed the fusion proteins, constructed the fusion protein cell lines, and designed and conducted the proteomics and biochemical analysis. SM supervised the structural studies, designed the PP1-substrate fusions, and conducted crystallography and AlphaFold3 modelling experiments. KE-B performed protein expression and crystallography. DJ designed and synthesised peptides. ROF and RT conceived the project, designed and interpreted experiments, and wrote the paper, with input from other authors.

Supplementary figure legends

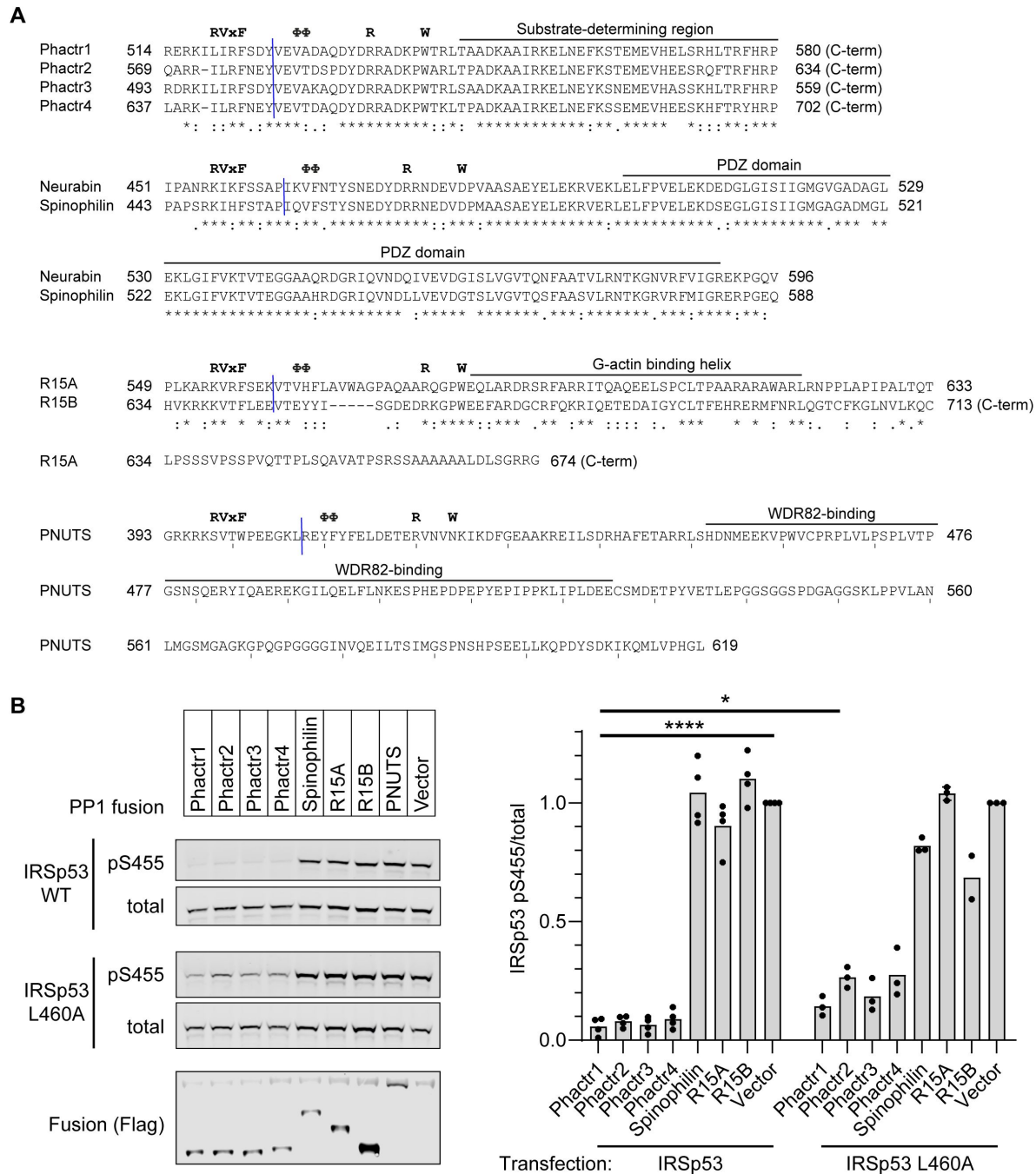


Figure S1.

A. PIP sequences in each fusion. Sequences of the PP1-binding and C-terminal sequences in each RVxF-ΦΦ-R-W PIP fusion are shown. Blue line indicates fusion point. Known interaction domains are overlined.

B. IRSp53 WT or L460A mutant were transfected into 293 Flp-In T-Rex cells expressing the different fusion proteins, induced by tetracycline. Immunoblotting for total and S455-phosphorylated IRSp53 is shown. Flag tag indicates expression of the fusion phosphatases. Quantification is at right.

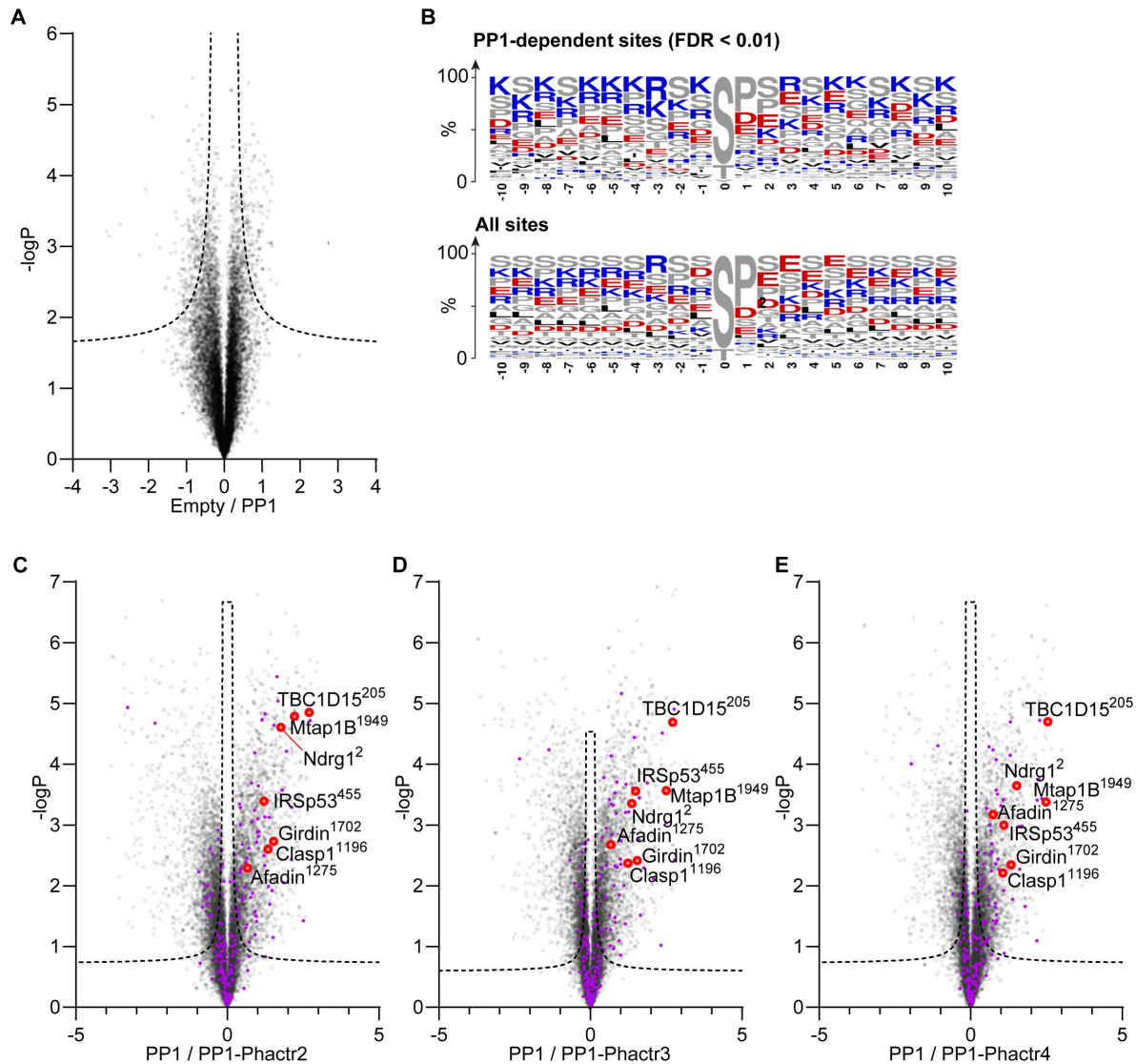


Figure S2.

A. Phosphorylation sites depleted in PP1-expressing samples compared with control empty-vector samples. Dashed line, 1% false-discovery rate cutoff.

B. Frequency plots for residues identified as PP1 hits in (A) and for all phosphorylation sites in the analysis. Enrichment is broadly consistent with published findings (Hoermann et al., 2020 [\[1\]](#)).

C-E. Phosphorylation sites depleted in PP1-Phactr2 (**C**), PP1-Phactr3 (**D**) and PP1-Phactr4 (**E**) fusion samples compared with PP1 samples. Purple - hits conforming to the Phactr1 substrate motif S/T-x_{2,3}-Φ-L. Red - top Phactr1/PP1 hits identified previously (Fedoryshchak et al., 2020 [\[2\]](#)).

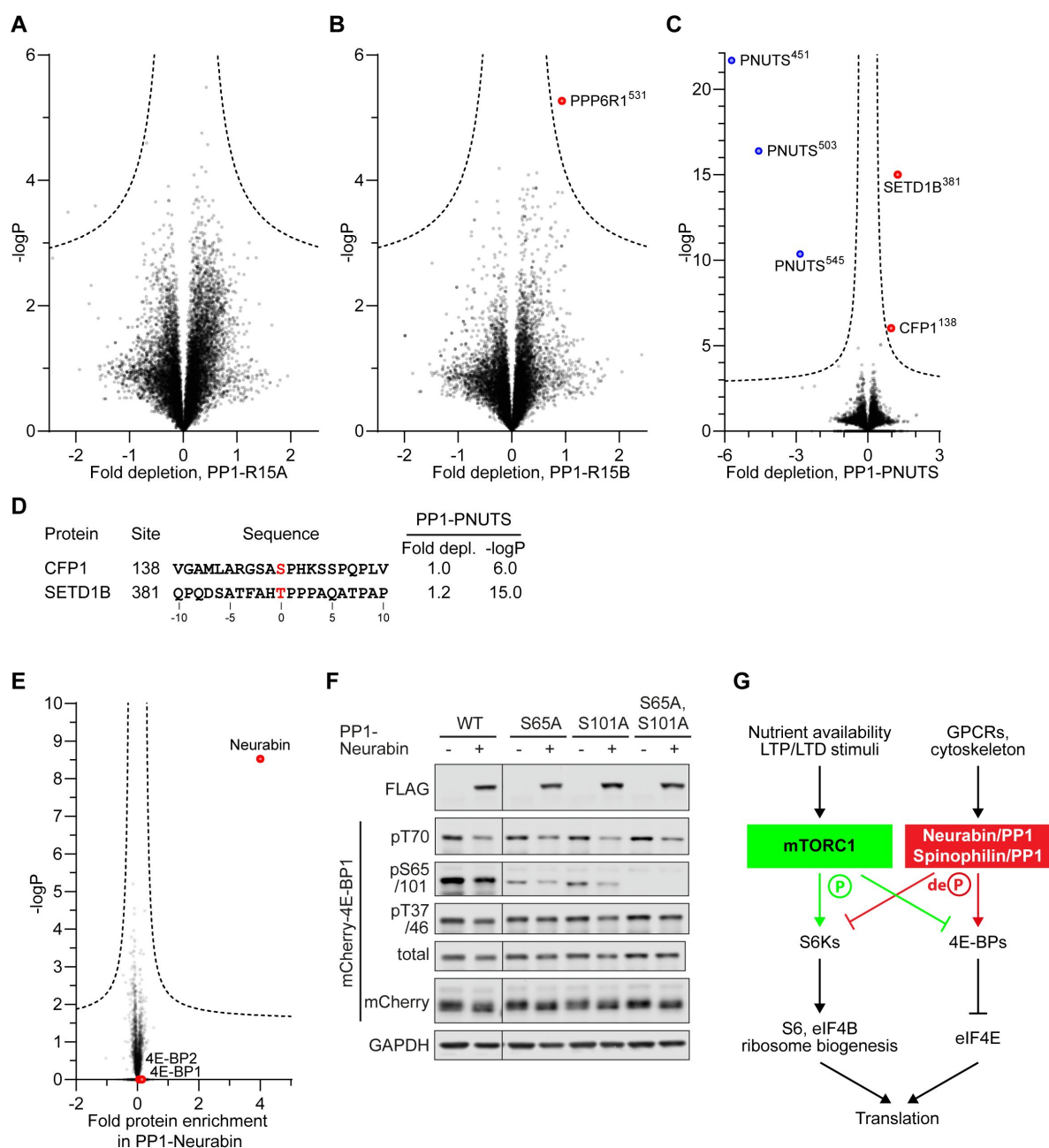


Figure S3.

A-C. Identification of PP1-R15A (**A**), PP1-R15B (**B**) and PP1-PNUTS (**C**) substrates by depletion of phosphorylation sites in the corresponding samples as opposed to average abundance in the dataset. Dashed line, 5% false-discovery threshold; red, significantly depleted phosphorylation sites; blue, PNUTS phosphorylation sites arising from overexpression of PP1-PNUTS.

D. Sequences of significantly depleted phosphorylation sites from PP1-PNUTS samples.

E. Comparison of total protein levels in cells PP1-Neurabin cells with or without induction. Neurabin and 4E-BPs are highlighted in red. Dashed line, 5% false-discovery threshold.

F. Specificity analysis of the commercial anti-phospho-S65 antibody.

G. mTORC1 pathway schematic (see (Hoeffer and Klann, 2010; Liu and Sabatini, 2020)).

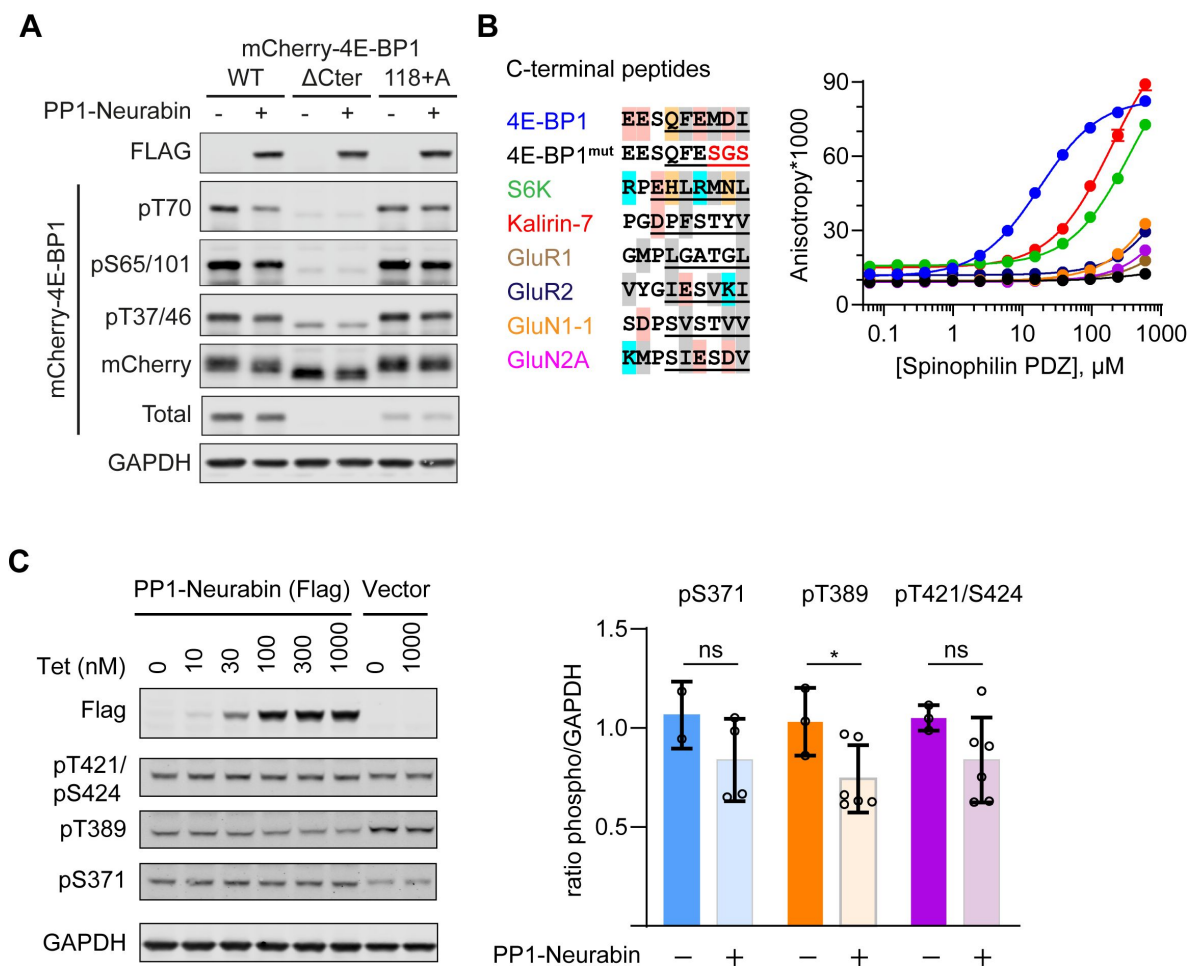


Figure S4.

A. Immunoblotting analysis of wildtype mCherry-4E-BP1 or mutants either lacking the 6 C-terminal residues (Δ Cter), or containing an additional C-terminal alanine (118+A) upon expression in 293 cells with or without PP1-Neurabin expression as indicated.

B. Left, sequence alignment of potential Neurabin/Spinophilin PDZ domain ligands.

Grey shading, hydrophobic residues; pink, acidic residues; cyan, basic residues; orange, hydrophilic residues. Underlining shows sequences N-terminally linked to 6-carboxyfluorescein (FAM) for use in fluorescence polarisation (FP) assay. FAM-labelled peptides were titrated with increasing concentrations of recombinant Spinophilin PDZ domain and affinity estimated from change in fluorescence anisotropy (for summary see **Figure 4C**).

C. Immunoblotting analysis of S6K phosphorylation 293 Flp-In T-Rex cells upon expression of PP1-Neurabin or empty vector.

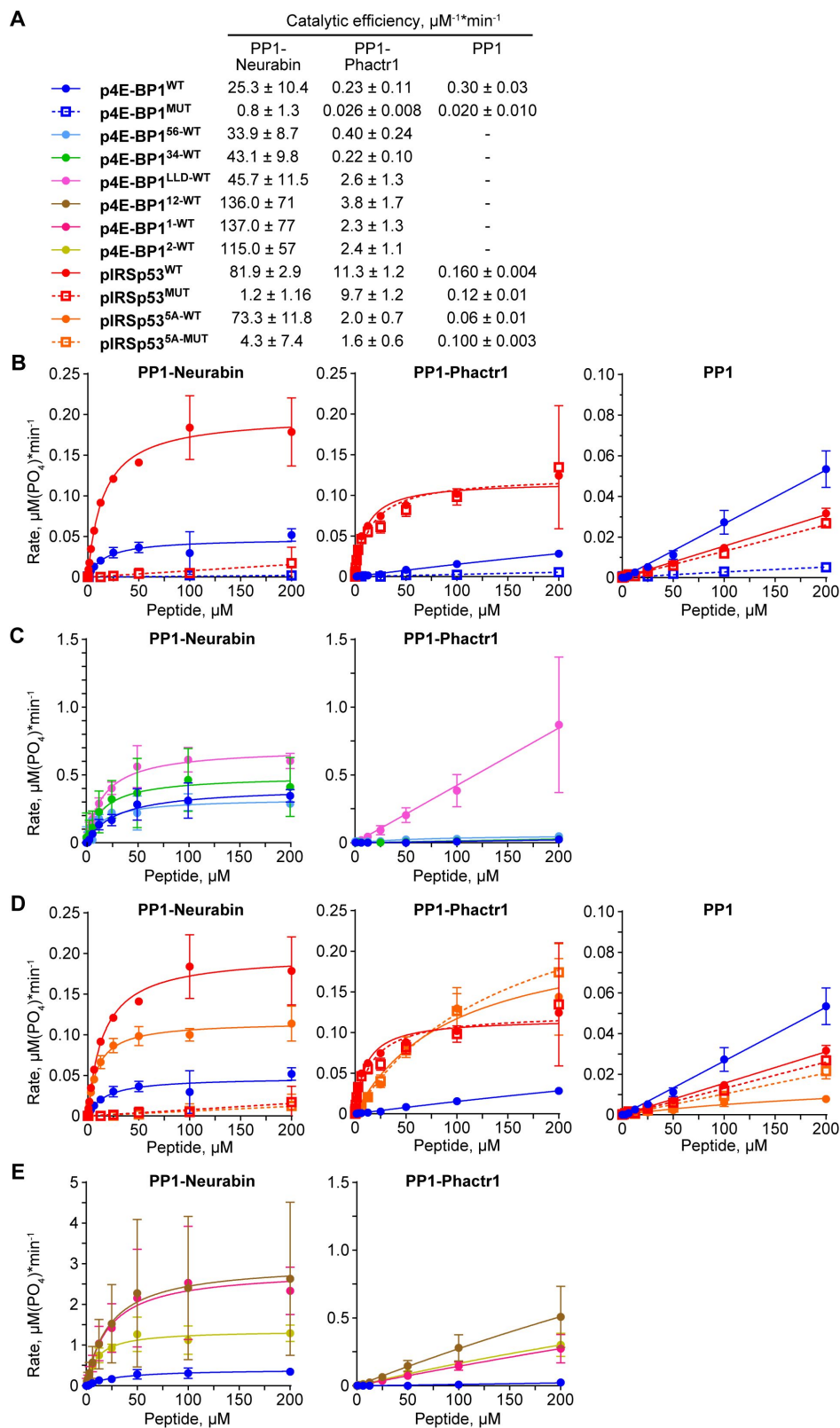


Figure S5.

A. Catalytic efficiencies for the various peptide dephosphorylation reactions by PP1-Neurabin, PP1-Phactr1 and PP1 are shown.

B-E. Dephosphorylation reaction rates plotted against substrate concentration for different sets of phosphopeptides with PP1-Neurabin, PP1-Phactr1 or PP1.

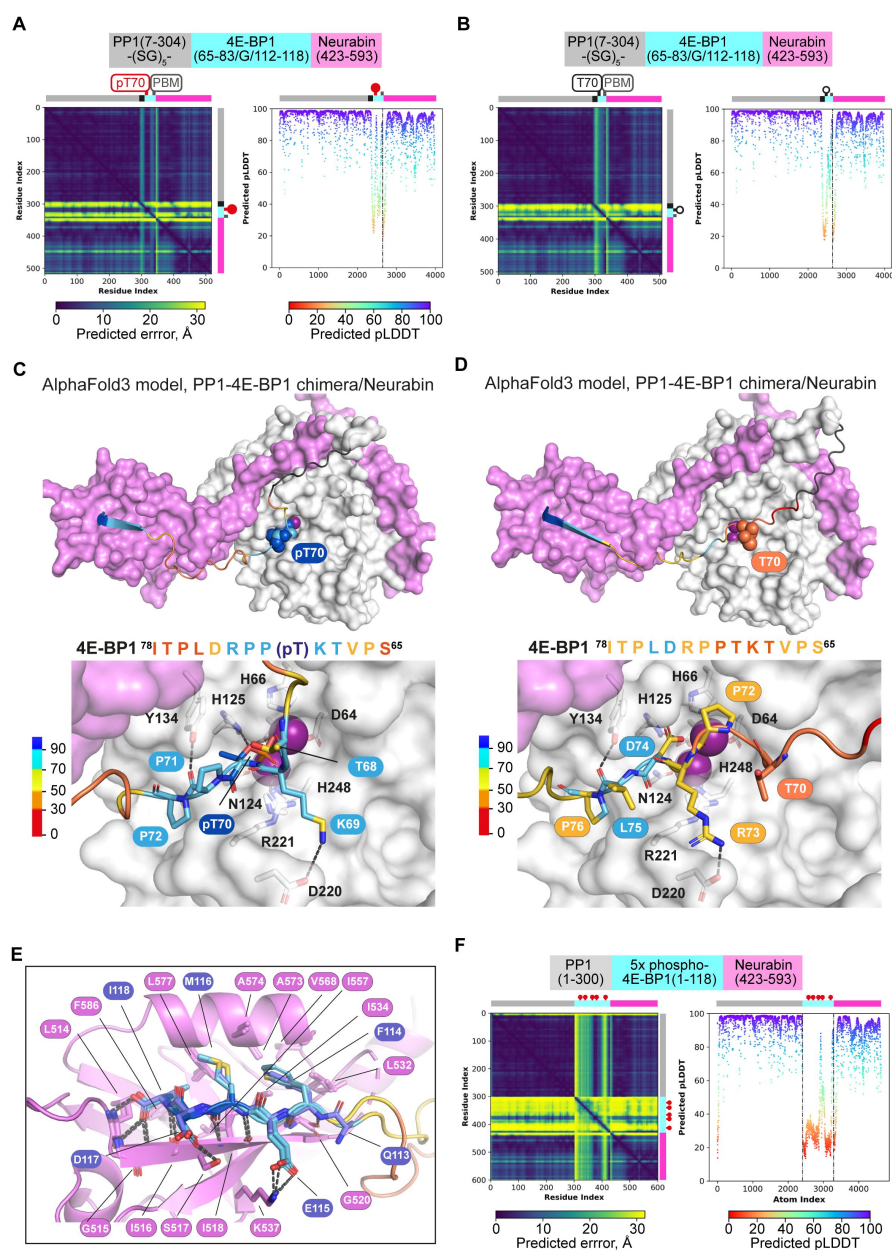


Figure S6.

A, B. AlphaFold3 models of the phosphorylated (A) and unphosphorylated (B) PP1-4E-BP1 chimera / Neurabin(423-593) interaction. Left, PAE plots; right, pLDDT plots, with confidence boundaries indicated by dashed lines (>90%, very high (side-chains); 70-90%, high (main-chain); 50-70%, low).

C, D. AlphaFold3 models of the phosphorylated (C) and unphosphorylated (D) PP1-4E-BP1 chimera / Neurabin(423-593) interaction. PP1 and Neurabin are shown respectively in white and lilac surface representation with PP1 active site Mn^{2+} ions in purple. 4E-BP1 sequences are in stick representation, colour coded according to the AlphaFold3 pLDDT score (inset), with pT70 and T70 in space-fill; linker residues are in black. Below are shown close-up views of predicted interactions with the PP1 catalytic site. For PAE and pLDDT plots, see A, B.

E. Comparison of crystal structure and AlphaFold3 model of 4E-BP1/PDZ interactions in phosphorylated and unphosphorylated PP1-4E-BP1 chimera / Neurabin(423-593) interaction. Predicted structures are oriented by superposition of the PDZ domain, shown in lilac ribbon representation. 4E-BP1 sequences are in stick representation, colour coded according to the AlphaFold3 pLDDT score (inset)

F. AlphaFold3 modelling of the Neurabin(423-593)/PP1 - 5x phospho-4E-BP1 interaction. Left, PAE plots; right, pLDDT plots, with confidence boundaries indicated by dashed lines (>90%, very high (side-chains); 70-90%, high (main-chain); 50-70%, low).

References

- Abramson J *et al.* (2024) **Accurate structure prediction of biomolecular interactions with AlphaFold 3** *Nature* **630**:493–500
- Adams PD *et al.* (2010) **PHENIX: a comprehensive Python-based system for macromolecular structure solution** *Acta Crystallogr D Biol Crystallogr* **66**:213–221
- Aguilar-Valles A, Matta-Camacho E, Khoutorsky A, Gkogkas C, Nader K, Lacaille JC, Sonenberg N (2015) **Inhibition of Group I Metabotropic Glutamate Receptors Reverses Autistic-Like Phenotypes Caused by Deficiency of the Translation Repressor eIF4E Binding Protein 2** *Neurosci* **35**:11125–11132
- Allen PB, Ouimet CC, Greengard P (1997) **Spinophilin, a novel protein phosphatase 1 binding protein localized to dendritic spines** *Proc Natl Acad Sci U S A* **94**:9956–9961
- Artemenko M, Zhong SSW, To SKY, Wong AST (2022) **p70 S6 kinase as a therapeutic target in cancers: More than just an mTOR effector** *Cancer Lett* **535**
- Bollen M, Peti W, Ragusa MJ, Beullens M (2010) **The extended PP1 toolkit: designed to create specificity** *Trends Biochem Sci* **35**:450–458
- Brautigan DL, Shenolikar S (2018) **Protein Serine/Threonine Phosphatases: Keys to Unlocking Regulators and Substrates** *Annu Rev Biochem* **87**:921–964
- Burnett PE, Blackshaw S, Lai MM, Qureshi IA, Burnett AF, Sabatini DM, Snyder SH (1998) **Neurabin is a synaptic protein linking p70 S6 kinase and the neuronal cytoskeleton** *Proc Natl Acad Sci U S A* **95**:8351–8356
- Casamayor A, Arino J (2020) **Controlling Ser/Thr protein phosphatase PP1 activity and function through interaction with regulatory subunits** *Adv Protein Chem Struct Biol* **122**:231–288
- Cenik BK, Shilatifard A (2021) **COMPASS and SWI/SNF complexes in development and disease** *Nat Rev Genet* **22**:38–58
- Chen R, Rato C, Yan Y, Crespillo-Casado A, Clarke HJ, Harding HP, Marciniak SJ, Read RJ, Ron D (2015) **G-actin provides substrate-specificity to eukaryotic initiation factor 2alpha holophosphatases** *Elife*
- Choy MS *et al.* (2014) **Understanding the antagonism of retinoblastoma protein dephosphorylation by PNUTS provides insights into the PP1 regulatory code** *Proc Natl Acad Sci U S A* **111**:4097–4102
- Cohen PT (2002) **Protein phosphatase 1--targeted in many directions** *J Cell Sci* **115**:241–256
- Cortazar MA, Sheridan RM, Erickson B, Fong N, Glover-Cutter K, Brannan K, Bentley DL (2019) **Control of RNA Pol II Speed by PNUTS-PP1 and Spt5 Dephosphorylation Facilitates Termination by a "Sitting Duck Torpedo" Mechanism** *Mol Cell* **76**:896–908

- Egloff MP, Cohen PT, Reinemer P, Barford D (1995) **Crystal structure of the catalytic subunit of human protein phosphatase 1 and its complex with tungstate** *J Mol Biol* **254**:942–959
- Emsley P, Lohkamp B, Scott WG, Cowtan K (2010) **Features and development of Coot** *Acta Crystallogr D Biol Crystallogr* **66**:486–501
- Erickson B *et al.* (2024) **PP1 PNUTS binds the “restrictor” and dephosphorylates RNA pol II CTD Ser5 to stimulate transcription termination** *Genes Dev*
- Fedoryshchak RO *et al.* (2020) **Molecular basis for substrate specificity of the Phactr1/PP1 phosphatase holoenzyme** *Elife*
- Foley K, McKee C, Nairn AC, Xia H (2021) **Regulation of Synaptic Transmission and Plasticity by Protein Phosphatase 1** *J Neurosci* **41**:3040–3050
- Goldberg J, Huang HB, Kwon YG, Greengard P, Nairn AC, Kuriyan J (1995) **Three-dimensional structure of the catalytic subunit of protein serine/threonine phosphatase-1** *Nature* **376**:745–753
- Harris BZ, Lim WA (2001) **Mechanism and role of PDZ domains in signaling complex assembly** *J Cell Sci* **114**:3219–3231
- Hoeffer CA, Klann E (2010) **mTOR signaling: at the crossroads of plasticity, memory and disease** *Trends Neurosci* **33**:67–75
- Hoermann B *et al.* (2020) **Dissecting the sequence determinants for dephosphorylation by the catalytic subunits of phosphatases PP1 and PP2A** *Nat Commun* **11**
- Holt CE, Martin KC, Schuman EM (2019) **Local translation in neurons: visualization and function** *Nat Struct Mol Biol* **26**:557–566
- Jones AW, Flynn HR, Uhlmann F, Snijders AP, Touati SA (2020) **Assessing Budding Yeast Phosphoproteome Dynamics in a Time-Resolved Manner using TMT10plex Mass Tag Labeling** *STAR Protoc* **1**
- Kelker MS, Dancheck B, Ju T, Kessler RP, Hudak J, Nairn AC, Peti W (2007) **Structural basis for spinophilin-neurabin receptor interaction** *Biochemistry* **46**:2333–2344
- Lee JH, You J, Dobrota E, Skalnik DG (2010) **Identification and characterization of a novel human PP1 phosphatase complex** *J Biol Chem* **285**:24466–24476
- Liu GY, Sabatini DM (2020) **mTOR at the nexus of nutrition, growth, ageing and disease** *Nat Rev Mol Cell Biol* **21**:183–203
- Liu J, Stevens PD, Eshleman NE, Gao T (2013) **Protein phosphatase PPM1G regulates protein translation and cell growth by dephosphorylating 4E binding protein 1 (4E-BP1)** *J Biol Chem* **288**:23225–23233
- Martineau Y, Azar R, Bousquet C, Pyronnet S (2013) **Anti-oncogenic potential of the eIF4E-binding proteins** *Oncogene* **32**:671–677
- McCoy AJ, Grosse-Kunstleve RW, Adams PD, Winn MD, Storoni LC, Read RJ (2007) **Phaser crystallographic software** *J Appl Crystallogr* **40**:658–674

- Novoa I, Zeng H, Harding HP, Ron D (2001) **Feedback inhibition of the unfolded protein response by GADD34-mediated dephosphorylation of eIF2alpha** *J Cell Biol* **153**:1011–1022
- Penzes P, Johnson RC, Sattler R, Zhang X, Hugarir RL, Kambampati V, Mains RE, Eipper BA (2001) **The neuronal Rho-GEF Kalirin-7 interacts with PDZ domain-containing proteins and regulates dendritic morphogenesis** *Neuron* **29**:229–242
- Ragusa MJ, Dancheck B, Critton DA, Nairn AC, Page R, Peti W (2010) **Spinophilin directs protein phosphatase 1 specificity by blocking substrate binding sites** *Nat Struct Mol Biol* **17**:459–464
- Romagnoli A, D’Agostino M, Ardiccioni C, Maracci C, Motta S, La Teana A, Di Marino D (2021) **Control of the eIF4E activity: structural insights and pharmacological implications** *Cell Mol Life Sci* **78**:6869–6885
- Sarrouilhe D, di Tommaso A, Metaye T, Ladeveze V (2006) **Spinophilin: from partners to functions** *Biochimie* **88**:1099–1113
- Schalm SS, Blenis J (2002) **Identification of a conserved motif required for mTOR signaling** *Curr Biol* **12**:632–639
- Subbaiah VK, Kranjec C, Thomas M, Banks L (2011) **PDZ domains: the building blocks regulating tumorigenesis** *Biochem J* **439**:195–205
- Tyanova S, Temu T, Sinitcyn P, Carlson A, Hein MY, Geiger T, Mann M, Cox J (2016) **The Perseus computational platform for comprehensive analysis of (prote)omics data** *Nat Methods* **13**:731–740
- Vaguine AA, Richelle J, Wodak SJ (1999) **SFCHECK: a unified set of procedures for evaluating the quality of macromolecular structure-factor data and their agreement with the atomic model** *Acta Crystallogr D Biol Crystallogr* **55**:191–205
- Ward RJ, Alvarez-Curto E, Milligan G (2011) **Using the Flp-In T-Rex system to regulate GPCR expression** *Methods Mol Biol* **746**:21–37
- Winter G, Lobley CM, Prince SM (2013) **Decision making in xia2** *Acta Crystallogr D Biol Crystallogr* **69**:1260–1273
- Wu LJ, Ren M, Wang H, Kim SS, Cao X, Zhuo M (2008) **Neurabin contributes to hippocampal long-term potentiation and contextual fear memory** *PLoS One* **3**
- Yan Y, Harding HP, Ron D (2021) **Higher-order phosphatase-substrate contacts terminate the integrated stress response** *Nat Struct Mol Biol* **28**:835–846
- Yan Z, Hsieh-Wilson L, Feng J, Tomizawa K, Allen PB, Fienberg AA, Nairn AC, Greengard P (1999) **Protein phosphatase 1 modulation of neostriatal AMPA channels: regulation by DARPP-32 and spinophilin** *Nat Neurosci* **2**:13–17
- Yang H, Jiang X, Li B, Yang HJ, Miller M, Yang A, Dhar A, Pavletich NP (2017) **Mechanisms of mTORC1 activation by RHEB and inhibition by PRAS40** *Nature* **552**:368–373

Author information

Roman O Fedoryshchak

Signalling and transcription Laboratory, Francis Crick Institute, London, UK

ORCID iD: [0000-0003-1865-8372](https://orcid.org/0000-0003-1865-8372)

Karim El-Bouri[^]

Structural Biology STP, Francis Crick Institute, London, UK

ORCID iD: [0000-0002-4542-0856](https://orcid.org/0000-0002-4542-0856)

[^]Present address: Protein Biogenesis Laboratory, Francis Crick Institute, London, UK

Dhira Joshi

Chemical Biology STP, Francis Crick Institute, London, UK

ORCID iD: [0000-0001-8660-2528](https://orcid.org/0000-0001-8660-2528)

Stephane Mouilleron

Structural Biology STP, Francis Crick Institute, London, UK

ORCID iD: [0000-0001-7977-6298](https://orcid.org/0000-0001-7977-6298)

Richard Treisman

Signalling and transcription Laboratory, Francis Crick Institute, London, UK

ORCID iD: [0000-0002-9658-0067](https://orcid.org/0000-0002-9658-0067)

For correspondence: Richard.Treisman@crick.ac.uk

Editors

Reviewing Editor

Jungsan Sohn

Johns Hopkins University School of Medicine, Baltimore, United States of America

Senior Editor

David Ron

University of Cambridge, Cambridge, United Kingdom

Reviewer #1 (Public review):

Summary:

In this manuscript the Treisman and colleagues address the question of how protein phosphatase 1 (PP1) regulatory subunits (or PP1-interacting protein (PIPs)) confer specificity on the PP1 catalytic subunit which by itself possesses little substrate specificity. In prior work the authors showed that the PIP Phactrs confers specificity by remodelling a hydrophobic groove immediately adjacent to the PP1 catalytic site through residues within the RVxF- \emptyset \emptyset -R-W string of Phactrs. Specifically, the residues proximal and including the 'W' of the RVxF- \emptyset \emptyset -R-W string remodel the hydrophobic groove. Other residues of the RVxF- \emptyset \emptyset -R-W string (i.e. the RVxF- \emptyset \emptyset -R) are not involved in this remodelling.

The authors suggest that the RVxF- $\emptyset\emptyset$ -R-W string is a conserved feature of many PIPs including PNUTS, Neurabin/spinophilin and R15A. However, from a sequence and structural perspective, only the RVxF- $\emptyset\emptyset$ -R- is conserved. The W is not conserved in most and in the R15A structure (PDB:7NZM) the Trp side chain points away from the hydrophobic channel - this could be a questionable interpretation due to model-building into the low-resolution cryo-EM map (4 Å).

In this paper, the authors convincingly show that Neurabin confers substrate specificity through interactions of its PDZ domain with the PDZ domain-binding motif (PBM) of 4E-BP. They show the PBM motif is required for Neurabin to increase PP1 activity towards 4E-BP and a synthetic peptide modelled on 4E-BP and also a synthetic peptide based on IRSp53 with a PBM added. The PBM of 4E-BP1 confers high affinity binding to the Neurabin PDZ domain. A crystal structure of a PP1-4E-BP1 fusion with Neurabin shows that the PBM of 4E-BP interacts with the PDZ domain of Neurabin. No interactions of 4E-BP and the catalytic site of PP1 are observed. Cell biology work showed that Neurabin-PP1 regulates the TOR signalling pathway by dephosphorylating 4E-BPs.

Strengths:

This work demonstrates convincingly using a variety of cell biology, proteomics, biophysics and structural biology that the PP1 interacting protein Neurabin confers specificity on PP1 through an interaction of its PDZ domain with a PDZ-binding motif of 4E-BP1 proteins. Remodelling of the hydrophobic groove of the PP1 catalytic subunit is not involved in Neurabin-dependent substrate specificity, in contrast to how Phactrs confers specificity on PP1. The active site of the Neurabin/PP1 complex does not recognise residues in the vicinity of the phospho-residue, thus allowing for multiple phospho-sites on 4E-BP to be dephosphorylated by Neurabin/PP1. This contrasts with substrate specificity conferred by the Phactrs PIP that confers specificity of Phactrs/PP1 towards its substrates in a sequence-specific context by remodelling the hydrophobic groove immediately adjacent to the catalytic. The structural and biochemical insights are used to explore the role of Neurabin/PP1 in dephosphorylation 4E-BPs in vivo, showing that Neurabin/PP1 regulates the TOR signalling pathway, specifically mTORC1-dependent translational control.

Weaknesses:

The only weakness is the suggestion that a conserved RVxF- $\emptyset\emptyset$ -R-W string exists in PIPs. The 'W' is not conserved in sequence and 3 dimensions in most of the PIPs discussed in this manuscript. The lack of conservation of the W would be consistent with the finding based on multiple PP1-PIP structures that apart from Phactrs, no other PIP appears to remodel the PP1 hydrophobic channel.

<https://doi.org/10.7554/eLife.103403.1.sa3>

Reviewer #2 (Public review):

This manuscript explores the molecular mechanisms that are involved in substrate recognition by the PP1 phosphatase. The authors previously showed that the PP1 interacting protein (PPI), PhactrI, conferred substrate specificity by remodelling the PP1 hydrophobic substrate groove. In this work, the authors aimed to understand the key determinant of how other PIPs, Neurabin and Spinophilin, mediate substrate recognition.

The authors generated a few PP1-PIP fusion constructs, undertook TMT phosphoproteomics and validated their method using PP1-Phactr1/2/3/4 fusion constructs. Using this method, the authors identified phosphorylation sites controlled by PP1-Neurabin and focussed their work on 4E-BP1, thereby linking PP1-Neurabin to mTORC1 signalling. Upon validating that PP1-

Neurabin dephosphorylates 4E-BP1, they determined that 4E-BP1 PBM binds to the PDZ domain of Neurabin with an affinity that was greater than 30-fold as compared to other substrates. PP1-Neurabin dephosphorylated 4E-BP1WT and IRSp53WT with a catalytic efficiency much greater than PP1 alone. However, PP1-Neurabin bound to 4E-BP1 and IRSp53 mutants lacking the Neurabin PDZ domain with a catalytic efficiency lesser than that observed with 4E-BP1WT. These results indicate the involvement of the PDZ domain in facilitating substrate recruitment by PP1-Neurabin. Interestingly, PP1-Phactr1 dephosphorylation of 4E-BP1 phenocopies PP1 alone, while PP1-Phactr1 dephosphorylates IRSp53 to a much higher extent than PP1 alone. These results highlight the importance of the PDZ domain and also shed light on how different PP1-PIP holoenzymes mediate substrate recognition using distinct mechanisms. The authors also show that the remodelling of the hydrophobic PP1 substrate groove which is essential for substrate recognition by PP1-Phactr1, was not required by PP1-Neurabin. Additionally, the authors also resolved the structure of a PP1-4E-BP1 fusion with the PDZ-containing C-terminal of Neurabin and observed that the Neurabin/PP1-4E-BP1 complex structure was oriented at 21{degree sign} to that in the unliganded Spinophilin/PP1 complex (resolved by Ragusa et al., 2010) owing to a slight bend in the C-terminal section that connects it to the RVxF-ΦΦ-R-W string. Since no interaction was observed with the remodelled PP1-Neurabin hydrophobic groove, the authors utilised AlphaFold3 to further answer this. They observed a high confidence of interaction between the groove and phosphorylated substrate and a low confidence of interaction between the groove and unphosphorylated substrate, thereby suggesting that the hydrophobic groove remodelling is not involved in PP1-Neurabin recognition and dephosphorylation of 4E-BP1.

In this work, the authors provide novel insights into how Neurabin depends on the interaction between its PDZ domain and PBM domains of potential substrates to mediate its recruitment by PP1. Additionally, they uncover a novel PP1-Neurabin substrate, 4E-BP1. They systematically employ phosphoproteomics, biochemical, and structural methods to investigate substrate specificity in a robust fashion. Furthermore, the authors also compare the interactions between PP1-Neurabin to 4E-BP1 and IRSp53 (PP1-Phactr1 substrate) with PP1-Phactr1, to showcase the specificity of the mode of action employed by these complexes in mediating substrate specificity. The authors employ an innovative PP1-PIP fusion strategy previously explored by Oberoi et al., 2016 and the authors themselves in Fedoryshchak et al., 2020. Although this method, allows for a more controlled investigation of the interactions between PP1-PIPs and its substrates, this methodology may not fully recapitulate the interactions that may occur in a physiological setting. This could potentially be overcome by studying the interactions of the full proteins using classical biochemical approaches in cell lines. Furthermore, the authors have substantially characterised the importance of the PDZ domain using their fusion constructs, however, I believe that further exploration into either structural or AlphaFold3 modelling of PBM domain substrate mutants, or a Neurabin PDZ-domain mutant might further strengthen this claim. Overall, the paper makes a substantial contribution to understanding substrate recognition and specificity in PP1-PIP complexes. The study's innovative methods, biological relevance, and mechanistic insights are strengths, but whether this mechanism occurs in a physiological context is unclear.

<https://doi.org/10.7554/eLife.103403.1.sa2>

Reviewer #3 (Public review):

Protein Phosphatase 1 (PP1), a vital member of the PPP superfamily, drives most cellular serine/threonine dephosphorylation. Despite PP1's low intrinsic sequence preference, its substrate specificity is finely tuned by over 200 PP1-interacting proteins (PIPs), which employ short linear motifs (SLIMs) to bind specific PP1 surface regions. By targeting PP1 to cellular sites, modifying substrate grooves, or altering surface electrostatics, PIPs influence substrate

specificity. Although many PIP-PP1-substrate interactions remain uncharacterized, the Phactr family of PIPs uniquely imposes sequence specificity at dephosphorylation sites through a conserved "RVxF-ΦΦ-R-W" motif. In Phactr1-PP1, this motif forms a hydrophobic pocket that favors substrates with hydrophobic residues at +4/+5 in acidic contexts (the "LLD motif"), a specificity that endures even in PP1-Phactr1 fusions. Neurabin/Spinophilin remodel PP1's hydrophobic groove in distinct ways, creating unique holoenzyme surfaces, though the impact on substrate specificity remains underexplored. This study investigates Neurabin/Spinophilin specificity via PDZ domain-driven interactions, showing that Neurabin/PP1 specificity is governed more by PDZ domain interactions than by substrate sequence, unlike Phactr1/PP1.

A significant strength of this work is the use of PP1-PIP fusion proteins to effectively model intact PP1•PIP holoenzymes by replicating the interactions that remodel the PP1 interface and confer site-specific substrate specificity. When combined with proteomic analyses to assess phospho-site depletion in mammalian cells, these fusions offer critical insights into holoenzyme specificity, revealing new candidate substrates for Neurabin and Spinophilin. The studies present compelling evidence that the PDZ domain of PP1-Neurabin directs its specificity, with the remodelled PP1 hydrophobic groove interactions having minimal impact. This mechanism is supported by structural analysis of the PP1-4E-BP1 substrate fusion bound to a Neurabin construct, highlighting the 4E-BP1/PDZ interaction. This work delivers crucial insights into PP1-PIP holoenzyme function, combining biochemical, proteomic, and structural approaches. It validates the PP1-PIP fusion protein model as a powerful tool, suggesting it may extend to studying additional holoenzymes. While an extremely useful model, it must be considered unlikely the PP1-PIP fusions fully recapitulate the specificity and regulation of the holoenzyme.

<https://doi.org/10.7554/eLife.103403.1.sa1>

Author response:

We are very pleased to see these positive reviews of our preprint.

Reviewers 1 and 3 raise issues around PIP-PP1 interactions.

| (1) Role of the "RVxF-ΦΦ-R-W string"

Most PIPs interact with the globular PP1 catalytic core through short linear interaction motifs (SLiMs) and Choy et al (PNAS 2014) previously showed that many PIPs interact with PP1 through conserved trio of SLiMs, RVxF-ΦΦ-R, which is also present in the Phactrs.

Previous structural analysis showed the trajectory of the PPP1R15A/B, Neurabin/Spinophilin (PPP1R9A/B), and PNUTS (PPP1R10) PIPs across the PP1 surface encompasses not only the RVxF-ΦΦ-R trio, but also additional sequences C-terminal to it (Chen et al, eLife, 2015). This extended trajectory is maintained in the Phactr1-PP1 complex (Fedoryshchak et al, eLife (2020). Based on structural alignment we proposed the existence of an additional hydrophobic "W" SLiM that interacts with the PP1 residues I133 and Y134.

The extended "RVxF-ΦΦ-R-W" interaction brings sequences C-terminal to the "W" SLiM into the vicinity of the hydrophobic groove that adjoins the PP1 catalytic centre. In the Phactr1/PP1 complex, these sequences remodel the groove, generating a novel pocket that facilitates sequence-specific substrate recognition.

This raises the possibility that sequences C-terminal to the extended "RVxF-ΦΦ-R-W string" in the other complexes also confer sequence-specific substrate recognition, and our study aims to test this hypothesis. Indeed, the hydrophobic groove structures of the

Neurabin/Spinophilin/PP1 and Phactr1/PP1 complexes differ significantly (Ragusa et al, 2010; see Fedoryshchak et al 2020, Fig2 FigSupp1).

| (2) *Orientation of the W side chain*

Reviewer 1 points out that in the substrate-bound PP1/PPP1R15A/Actin/eIF2 pre-dephosphorylation complex the W sidechain is inverted with respect to its orientation in PP1-PPP1R15B complex (Yan et al, NSMB 2021). The authors proposed that this may reflect the role of actin in assembly of the quaternary complex. This does not necessarily invalidate the notion that sequences C-terminal to the “W” motif might play a role in actin-independent substrate recognition, and we therefore consider our inclusion of the R15A/B fusions in our analysis to be reasonable.

| (3) *Conservation of W*

The motif ‘W’ does not mandate tryptophan - Phactrs and PPP1R15A/B indeed have W at this position but Neurabin/spinophilin contain VDP, which makes similar interactions. Similarly the “_RVxF” motifs in Phactr1, Neurabin/Spinophilin, PPP1R15A/B and PNUTS are LIRF, KIKF, KV(R/T)F and TVTW respectively.

In our revision, we will present comparisons of the differentially remodelled/modified PP1 hydrophobic groove in the various complexes, discuss the different orientations of the tryptophan in the previously published PPP1R15A/PP1 and PPP1R15B/PP1 structures. We will also address the other issues raised by the referees.

<https://doi.org/10.7554/eLife.103403.1.sa0>